Nucleic Acids Research, 2020 **1**
doi: 10.1093/nar/gkaa758

Readthrough of stop codons under limiting ABCE1 concentration involves frameshifting and inhibits nonsense-mediated mRNA decay

Giuditta Annibaldis[1,2,†], Michal Domanski[1,†], René Dreos[3], Lara Contu[1,2], Sarah Carl[4], Nina Kläy[1] and Oliver Mühlemann[1,*]

[1]Department of Chemistry and Biochemistry, University of Bern, Freiestrasse 3, CH-3012 Bern, Switzerland, [2]Graduate School for Cellular and Biomedical Sciences, University of Bern, Mittelstrasse 43, CH-3012 Bern, Switzerland, [3]Center for Integrative Genomics, University of Lausanne, CH-1015 Lausanne, Switzerland and [4]Friedrich Miescher Institute for Biomedical Research, Maulbeerstrasse 66, CH-4058 Basel, Switzerland

Received January 09, 2020; Revised August 28, 2020; Editorial Decision August 31, 2020; Accepted September 09, 2020

ABSTRACT

To gain insight into the mechanistic link between translation termination and nonsense-mediated mRNA decay (NMD), we depleted the ribosome recycling factor ABCE1 in human cells, resulting in an upregulation of NMD-sensitive mRNAs. Suppression of NMD on these mRNAs occurs prior to their SMG6-mediated endonucleolytic cleavage. ABCE1 depletion caused ribosome stalling at termination codons (TCs) and increased ribosome occupancy in 3′ UTRs, implying enhanced TC readthrough. ABCE1 knockdown indeed increased the rate of readthrough and continuation of translation in different reading frames, providing a possible explanation for the observed NMD inhibition, since enhanced readthrough displaces NMD activating proteins from the 3′ UTR. Our results indicate that stalling at TCs triggers ribosome collisions and activates ribosome quality control. Collectively, we show that improper translation termination can lead to readthrough of the TC, presumably due to ribosome collisions pushing the stalled ribosomes into the 3′ UTR, where it can resume translation in-frame as well as out-of-frame.

INTRODUCTION

Translation, the synthesis of proteins by ribosomes according to the genetic information stored in messenger RNA (mRNA), is a central process in all forms of life. Although absolutely essential and hence requiring a high level of precision, translation involves many different factors that need to interact and function in a complex and highly orchestrated manner, and mistakes can occur at essentially every step. To achieve the necessary precision, cells have evolved numerous mechanisms to assess the integrity of mRNA and aberrancies in the functioning of ribosomes during translation (1,2). In eukaryotes, nonsense-mediated mRNA decay (NMD) is one of these translation-dependent quality control pathways that degrades mRNAs that fail to properly terminate translation (3). In the past, NMD was believed to target and degrade exclusively mRNAs carrying an aberrant premature termination codon (PTC) that interrupts the open reading frame (ORF), thereby suppressing the production of potentially deleterious C-terminally truncated proteins (4). However, with the advent of transcriptome-wide profiling methods it became clear that NMD regulates the levels of 5–10% of all mRNAs, the vast majority of them encoding perfectly functional full-length proteins (5–11). In the majority of these endogenous NMD targeted transcripts, there is a termination codon (TC) located >50 nucleotides upstream of the 3′-most exon-exon junction, a constellation that has been known for a long time to trigger NMD (12). Besides TCs located >50 nucleotides upstream of the 3′-most exon–exon junction, which can result from alternative pre-mRNA splicing, the presence of upstream open reading frames (uORFs), selenocysteine codons read as termination codons under low selenocysteine conditions, or the presence of introns in the 3′ untranslated region (3′ UTR), long 3′ UTRs have also been documented to trigger NMD (11,13–15). Generally, the mRNA levels of NMD targeted transcripts with exon-exon junctions in the 3′ UTR are reduced by NMD to a greater extent than those with a long 3′ UTR, suggesting that exon junction complexes (EJCs) residing in the 3′ UTR of an NMD-sensitive mRNA act as enhancers of NMD (16). EJCs are multiprotein complexes deposited 20–24 nucleotides upstream of exon-exon junctions during pre-mRNA splicing (17,18) and removed from the coding sequence during translation (19), leaving

*To whom correspondence should be addressed. Tel: +41 31 631 4627; Email: oliver.muehlemann@dcb.unibe.ch
†The authors wish it to be known that, in their opinion, the first two authors should be regarded as Joint First Authors.

behind only EJCs in the 3′ UTR on mRNAs undergoing translation. Notably, the transcriptome-wide studies also revealed that many Pol II transcripts annotated as long non-coding RNAs are targeted by NMD (5), in accordance with ribosome profiling studies showing that they in fact engage with ribosomes that translate short ORFs present in these transcripts (20–22).

The exact mechanism determining which RNAs will be targeted by NMD and which ones will be spared is subject to intense research and not yet well understood. The currently available data indicates that NMD ensues when a ribosome stalls at a termination codon (TC) for prolonged time because of a failure to properly or fast enough terminate translation (23,24). On mRNA with problems in translation termination, the so-called SURF complex (composed of SMG1, UPF1 and the release factors eRF1 and eRF3) was proposed to assemble at the TC (15,25,26). SMG1-mediated phosphorylation of UPF1, a core factor of NMD, appears to be a key event in activating NMD, because hyper-phosphorylated UPF1 subsequently serves as a binding platform for the heterodimer SMG5/SMG7 and for the endonuclease SMG6, allowing for two different decay routes (27). A third decay pathway operating via SMG5 and PNRC2 has also been proposed (28) but remains controversial (29,30). Moreover, a recent study challenged the SURF complex-based NMD activation model by showing that UPF3B rather than UPF1 interacts with the release factors (31).

While EJC-enhanced NMD appears to be vertebrate-specific, extended 3′ UTR length has been reported as an NMD-inducing feature in a wide range of eukaryotes (13–15,32,33). Consistent with the idea that ribosomes may fail to properly terminate translation when located too far away from the poly(A) tail, tethering of poly(A)-binding protein (PABP) nearby NMD-inducing TCs suppressed NMD in *Saccharomyces cerevisae*, *Drosophila melanogaster* and mammalian cells (14,15,23,25,34,35).

Prolonged ribosome stalling at NMD-inducing TCs increases the probability of readthrough, triggered by the accommodation of a near-cognate tRNA into the ribosome A-site, which then in turn can inhibit NMD (36,37), presumably by stripping off the 3′ UTR NMD activators (e.g. UPF1, EJC) (36). Frequent readthrough was shown to displace 3′ UTR-associated UPF1 from the mRNA, while inefficient readthrough allowed UPF1 (re-)association but blocked the initiation of mRNA decay at a subsequent rate-limiting step (36). Although translation termination is generally kinetically favored over readthrough, the interaction between the TC and eRF1 is dependent on the nucleotide context, the eRF1 concentration and the availability of other factors needed for translation termination (38). Besides the GTPase eRF3, the ribosome recycling factor ABCE1, an ATPase belonging to the ATP-binding cassette (ABC) protein family, plays crucial role in translation termination (39). When an elongating ribosome arrives at a TC, eRF1 together with GTP-bound eRF3 binds the A-site of the ribosome. After eRF1-mediated hydrolysis and release of the nascent polypeptide chain from the tRNA in the P-site, ABCE1 interacts with eRF1 and promotes the splitting of the two ribosomal subunits and the release of the mRNA from the small subunit, providing the functional link between translation termination and a new round of translation initiation (40,41). Several studies in different organisms demonstrated that silencing of ABCE1 affects the entire translation cycle and protein homeostasis of the cell (42–45). In particular, the loss of ABCE1 led to increased ribosome stalling at TCs in an *in vitro* reconstituted translation system (46) and to the accumulation of post-terminating ribosomes in the 3′UTR of mRNAs in erythroid cells (47).

Much progress has recently been made in understanding the molecular mechanism by which ribosome-associated quality control (RQC) recognizes ribosome stalling at specific sites in the ORF, triggering degradation of the nascent polypeptides and mRNAs (48–50). The collided di-ribosome (disome) is the structural entity recognized by the E3 ubiquitin ligase Hel2/ZNF598 (49,51). After binding of Hel2/ZNF598 to disomes, specific ribosomal proteins become ubiquitinated, which in turn activates downstream quality control events (52–54). While the majority of examples about ZNF598's role in RQC activation stem from ribosomes stalled on a poly(A) stretch or at the 3′-end of a truncated mRNA, ribosome collisions have recently also been detected in the context of aberrant translation termination *in vitro* and under various types of ribosome stalls *in vivo* (51), suggesting a more general role for ZNF598 in the recognition of aberrant translation events and in preventing the production of faulty proteins. Indeed, in the absence of the no-go mRNA surveillance pathway (NGD), increased ribosome collisions and +1 frameshifting was observed in yeast (55).

To gain more insight into the mechanistic links between translation termination and NMD, we investigated the effect of ABCE1 silencing on NMD. Here, we provide evidence that depletion of ABCE1 in HeLa cells not only leads to stalling of ribosomes at TCs but concomitantly also increases the rate of readthrough on these mRNAs. On many NMD-sensitive mRNAs, this increased readthrough suppresses NMD, consistent with the evidence that the ribosomes that translate into the 3′ UTR may prevent NMD by displacing NMD factors from these transcripts (36). Furthermore, we also demonstrate that the absence of proper ribosome recycling can cause a pileup of ribosomes on mRNAs with high translation rates, which increases the chance of following ribosomes bumping into ribosomes stalled at the TC, pushing them into the 3′ UTR where they can resume translation in-frame as well as out-of-frame.

MATERIALS AND METHODS

Cell culture and transfection

HeLa cells were cultured in DMEM supplemented with 10% fetal calf serum (FCS) and antibiotics. Cells were grown in 5% CO_2 at 37°C. HeLa cells stably expressing TCRβ and the Ig-μ reporter genes were described previously (56,57). For readthrough experiments, cells were treated with 400 μg/ml G418 (Fisher Scientific) for 24 h before harvesting. SiRNA-mediated knockdowns were carried out by a double-transfection procedure. First, 3×10^5 HeLa cells per well were seeded in six-well plates. One day later, the cells were transfected with 52 pmol of siRNA

using Lullaby reagent (OZ Biosciences). After 2 days, the cells were re-transfected as before. Protein and total RNA were isolated after one additional day. SiRNAs with the sequence 5′-GAGGAGAGUUGCAGAGAUUU-3′, HSS10985 and HSS10986 (Invitrogen) for targeting ABCE1 and 5′-GAUGCAGUUCCGCUCCAUU-3′ for targeting UPF1 were used. Readthrough assays were performed using the p2luc plasmids as described previously (25). Briefly, 3×10^5 HeLa cells per well were seeded in six-well plates. One day later, the cells were transfected with 52 pmol of siRNA using Lullaby reagent (OZ Biosciences). After 2 days, the cells were re-transfected with 52 pmol of siRNA and 800 ng of the indicated plasmids using Lipofectamine 2000 (Invitrogen). Protein and total RNA were isolated after two additional days. p2luc plasmids to assess readthrough combined with frameshift (p2luc + 1) were generated by site mutagenesis introducing an adenosine downstream the stop codon (UAA, UAG or UGA) between the two luciferases ORFs, and experiments with these new reporters were performed as before.

Knockdown efficiencies of the different targets were verified by western blotting using anti-ABCE1 (Abcam, ab185548), anti-Tyrosine Tubulin (Tub1A2) (Sigma, T9028), anti-RPS3 (Bethyl A303-840A), anti-RPL4 (proteintech, 11302-1-AP), anti-RACK1 (bethyl A302-545A), anti-RPS27A [(58) a kind gift of U. Kutay], anti-GFP (SicGen, AB0020-500) and anti-CPSF100 (custom made) antibodies. For IgM-μ protein detection, anti-IgM-μ (Jackson Imm. 115-005-020) was used in combination with Pierce Western Blot Signal Enhancer kit (Thermo Scientific).

Luciferase assay for readthrough quantification

Dual luciferase assays were performed according to the manufacturer's protocol (Promega). Luminescence was measured using TECAN Infinite M1000, two technical replicates for each sample. Readthrough efficiency was calculated by comparing the ratio of Firefly to Renilla luciferase activity relative to the plasmid without stop codon.

Puromycin incorporation assay

Translation level analysis was performed using an adapted protocol from a previous study (59). Briefly, HeLa cells were labeled with 10 μg/ml of puromycin (Santa Cruz) for 10 min in complete medium. After 30 min in puromycin free medium, cells were harvested and puromycin incorporation was detected by immunoblotting using a specific anti-puromycin-12D10 antibody (Millipore, MABE343). The western blot signal was quantified using the ImageJ program and displayed as mean ± standard deviation (SD). Student's *t* test was used to determine *P*-values.

Detection of out-of-frame readthrough product

ABCE1 knockdown using HSS10985 siRNA was performed as above. On day 4, cells were co-transfected with HSS10985 siRNA and pcDNA5/FRT/TO plasmid encoding for eGFP and C-terminal FLAG tag in 0 frame and SPOT tag in +1 frame using Lipofectamine2000. 24 h later, cells were harvested and resuspended in 500 μl lysis buffer (150 mM NaCl, 50 mM HEPES, pH 7.4, 0.5% Triton X-100, protease inhibitors). Cell lysate was sonicated 3 × 10 s, amp 45 (Vibra-Cell sonicator) and clarified by centrifugation (16 100 × rcf for 10 min at 4°C). The supernatant was incubated either with anti-SPOT beads (SpotTrap magnetic agarose, Chromotek), or anti-FLAG beads (M2 antibodies coupled to Dynabeads M-270 Epoxy) to immunoprecipitate the out-of-frame or in-frame readthrough products, respectively. eGFP was immunoprecipitated using GFP-Trap magnetic agarose (Chromotek). In all cases, bound proteins were eluted in protein loading buffer and analyzed by western blotting using the indicated antibodies.

RNA manipulations and analysis

RNA was extracted using TriReagent according to the manufacturer's instructions. RT-qPCR analyses were performed using Brilliant III Ultra-Fast SYBR® Green (Agilent) after DNase treatment using Turbo DNase (AMBION). All primers used in this study are listed in Supplementary Table S1. Data are displayed as mean ± SD. Student's *t* test was used and n values are indicated in the respective figure legends. GraphPad Prism v8 was used to create plots. For the analysis of total RNA by RNA-seq, rRNA-depleted mRNA was purified and used for library preparation using TruSeq Stranded mRNA Library Prep Kit (Illumina) and sequenced with Illumina HiSeq2500. Northern blot analysis was performed according to an adapted protocol from a previous study (60). Briefly, ∼10 μg RNA per sample was separated on a 1.2% (w/v) agarose gel containing 1× MOPS and 1% (v/v) formaldehyde and transferred to a positively charged nylon membrane by wet transferring. The ^{32}P-labeled ribo-probe was hybridized in ULTRAHyb buffer (AMBION) at 68°C overnight. The ribo-probes were transcribed from a NotI digested plasmids using SP6 polymerase (Fisher) in the presence of α^{32}P-UTP. The ribo-probe sequences are listed in Supplementary Table S1.

Polysome fractionations

The polysome profiling protocol was adapted from (61). Briefly, HeLa cells, with or without knockdown (two 150-mm culture dishes per condition) were treated with 100 μg/ml cycloheximide (Focus biomolecules) for 4 min at 37°C. Cells were then lysed in low-salt buffer (10 mM Tris–HCl [pH 7.5], 10 mM NaCl, 10 mM $MgCl_2$, 1 mM DTT, 1% Triton X-100, 1% Na-deoxycholate) supplemented with RNAse Inhibitor (NxGen), Protease Inhibitor cocktail (Biotools) and 100 μg/ml cycloheximide by quickly vortexing. After 2 min on ice, lysates were cleared by centrifugation for 5 min at 16 000 g. Lysates were loaded on 15–50% sucrose gradient tube and centrifuged at 40 000 rpm in a Beckman SW-41Ti rotor for 2 h at 4°C. Gradients were fractionated and monitored at absorbance 254 nm with a fraction collector (BioComp Instruments) at a 0.2-mm/s EM1 speed, with a distance of 3.71 mm per fraction. RNA was precipitated from gradient fractions with 3 volumes of 100% ethanol (overnight at −80°C). The next day, samples were centrifuged for 15 min at 16 000 g (4°C). Resulting pellets were reconstituted in 1 ml of TriReagent. RNA was precipitated from the aqueous fraction with isopropanol (–20°C,

overnight). Proteins were precipitated from gradient fractions with 0.1 volume of 100% TCA and 1 volume of acetone (overnight at −80°C). The volumes of the monosome and disome fractions used for the protein analysis shown in Figure 6 were adjusted based on the OD 260 nm values (rRNA) to achieve equal overall protein amounts. The next day, samples were centrifuged for 15 min at 16 000 g (4°C). Resulting pellets were additionally washed 3 × 1 ml ice-cold acetone, followed by centrifugation for 5 min at 16 000 g (4°C). After the last wash, pellets were dried in a vacuum concentrator (Eppendorf, 15 min, no heating, no brake, V-HV vacuum high vapor program). Prior to mass spectrometric analysis, dried pellets were reconstituted in 8 M urea, 100 mM Tris pH 8, reduced, alkylated and digested with trypsin. For the western blot, pellets were reconstituted in 1.5× LDS, 50 mM DTT loading buffer.

AHA-labeling click-it experiment

Newly synthesized proteins were labeled with 40 μM L-azidohomoalanine (AHA, ThermoFisher C10102) under ABCE1 knockdown or control condition for 90 min in methionine-free medium at 37°C. Before starting the labeling, cells were pre-incubated in methionine-free medium for 30 min at 37°C. Labeled proteins were assessed using tetramethylrhodamine (TAMRA) protein analysis detection kit (ThermoFisher C33370). Labeled proteins were analyzed using SDS-PAGE and direct imaging using a gel doc system equipped with appropriate fluorescent filter. Additionally, to control for an equal loading, the gel was subsequently stained with SYPRO Ruby protein stain (ThermoFisher S12001). For the mass spectrometric analysis, newly synthesized labeled proteins were captured using Click-iT Protein Enrichment Kit (ThermoFisher C10416). Captured AHA-labeled proteins were digested with trypsin and characterized using mass spectrometry. All the procedures including AHA labeling and click-it chemistry were carried out accordingly to the manufacturer's instructions.

Ribosome profiling experiments

Cells for ribosome profiling and RNA sequencing were processed using an adapted protocol from previous publications (62,63). Cells were washed with ice-cold phosphate buffered saline (PBS) and flash-frozen in liquid nitrogen. Subsequently, cells were scraped and lysed in lysis buffer (20 mM Tris–HCl pH7.4, 150 mM NaCl, 5 mM $MgCl_2$, 1% Triton X-100, 1 mM DTT, 25 U/ul Turbo DNase, Turbo DNase buffer) on ice. Next, cells were triturated ten times through a 27-gauge needle of a syringe and clarified by centrifugation. For ribosome profiling, lysates (about 4 U_{260}) were subsequently treated with 200 U RNase I (Ambion) for 10 min at 23°C and shaking at 300 rpm. The digestion was stopped by addition of 100 U SUPERase In RNase inhibitor (Ambion). Monosomes were separated on Illustra Micro-Spin S-400 HR gel filtration columns (GE Healthcare Life Science) as previously described (62). TriReagent was added immediately to the eluates and samples were stored at −80°C until further processing. RNA was isolated according to the TriReagent protocol and separated on 15% Novex polyacrylamide gels (Invitrogen). Ribosome footprints were excised between 26 and 34 nucleotide RNA size markers. After RNA isolation and purification, rRNAs were removed using the RiboZero kit (Illumina) according to manufacturer's datasheet. Sequencing libraries from ribosome footprints were generated as previously described (62). RNA-seq libraries were prepared from cells lysed similar as the ribosome profiling samples. RNA was isolated from cleared lysates by addition of TriReagent as for the ribosome-protected fragments (see above). Total RNA was used for library generation with the TruSeq Stranded mRNA Library Prep Kit (Illumina) according to the manufacturer's instructions. Libraries were sequenced on an Illumina HiSeq2500 generating 100 nt single-end reads.

RNA-sequencing analysis

The human transcriptome annotation was downloaded from the Ensemble database, using version GRCh38.p10. Both transcripts annotated as coding and as non-coding RNAs were included in the reference. Reads were mapped to the reference transcriptome and transcript abundance was quantified using Salmon (64). Estimated transcript counts were imported into R using the tximport package (65). Transcripts with more than eight counts in at least three independent samples were kept for further analysis. For correlation and plotting, transcript counts were normalized by scaling to the mean of total counts across samples, then $\log_2$-transformed after adding a pseudocount of 8. EdgeR was used for differential expression analysis (66), with raw, non-normalized counts as inputs. A likelihood-ratio test was used to determine differentially expressed genes.

Ribosome profiling analysis

The raw reads of the ribosome profiling experiments were trimmed based on quality and sequence adapters removed with Cutadapt v.1.8 (67). Reads with the expected read length (16–35 nt for the ribosome footprint (RPF) and 35–60 nt for total RNA) were kept for further analysis. Reads mapping *Homo sapiens* ribosomal RNA (rRNA) and transfer RNA (tRNA) databases (ENSEMBL v91) (68) using to bowtie2 (v.2.3.4.1) (69) were excluded. The remaining reads were aligned against *H. sapiens* transcripts database (ENSEMBL v91) using bowtie2 (v.2.3.4.1). Multi-mapping reads were filtered out and the remaining reads summarized at a gene level using an in-house script. Ribosome density (also called translational efficiency) was calculated in R (v.3.6.1). Raw genes ribosome footprints and total RNA counts were normalised using the DESeq2 package (70). Functional enrichment analysis (i.e. KEGG) was performed using the R packages biomaRt (71) and reactomePA (72). Read distribution analysis around termination codons was performed at transcript level, following a recently described strategy (73). To minimize the probability of falsely assigning RPFs originating from overlapping CDSs to stop codons and 3′ UTRs of related transcript isoforms of the same gene, one transcript was selected for each gene by applying the following selection criteria consecutively: (i) protein-coding genes must not overlap; (ii) select transcripts with the most downstream stop codon; (iii) select transcripts with the highest APPRIS score (74); (iv) for

the few still non-unique cases (874 out of 12401 expressed genes), select one randomly. Heat-maps were performed using the ChIP-Extract tool from the ChIP-Seq toolkit (75). Subsequently, the 5′-end of each RPF read for the selected transcripts was shifted 15 bases downstream to represent the ribosome A site. Selected transcripts were then sorted according to the total number of ribosome A sites mapping in the stop codon, or 100 nucleotides downstream the termination codon.

RESULTS

Knockdown of the ribosome recycling factor ABCE1 renders many endogenous NMD targets immune to NMD

Based on previous work indicating a link between translation termination and NMD [reviewed in (3)], we hypothesized that interfering with translation termination would alter the abundance of many mRNAs, in particular NMD-sensitive transcripts. To test this hypothesis and identify the affected genes, we established an siRNA-based knockdown protocol that enabled us to reduce the protein level of the ribosome recycling factor ABCE1 to ∼10% in HeLa cells (Figure 1A). In three biological replicates, total RNA isolated from cells with an ABCE1 knockdown (ABCE1 KD) or cells with a control knockdown (CTRL KD) was depleted for rRNA, reverse transcribed and subjected to high throughput Illumina sequencing (RNA-seq) to assess the steady-state levels of mRNAs transcriptome-wide. Comparison of the three ABCE1 KD datasets among each other and with the three Ctrl KD datasets revealed an overall high correlation (Pearson correlation coefficients between 0.78 and 0.91), demonstrating not only good reproducibility among the biological replicates, but also indicating that ABCE1 KD does not cause a global change in RNA levels (Supplementary Figure S1). Of the totally detected 47 830 transcripts, 3722 (7.8%) changed by 2-fold or more and with a P-value ≤ 0.05 (Figure 1B). The detected changes occurred to a similar extent in both directions, with 1757 up- and 1965 down-regulated transcripts. Notably, prolonged depletion of ABCE1 reduces cell proliferation based on observing ∼30% less cells in cultures transfected with ABCE1-targeting siRNAs compared to control siRNAs.

To assess the effect of ABCE1 KD on NMD-sensitive transcripts, we used a previously identified high-confidence set of endogenous NMD targeted genes (5). This list comprises about 1000 NMD targets that were identified based on their RNA level increase in UPF1, SMG6 and SMG7 knockdowns, as well as their decrease in the respective rescue experiments (5). Of the 644 high-confidence NMD targets that we could detect in our analysis here, 109 (16.9%) changed significantly (P-value ≤ 0.05) by 2-fold or more upon ABCE1 KD, with the vast majority (96 transcripts) being upregulated (Figure 1B, red and green dots). Thus, compared to non-NMD targets, the NMD-sensitive transcripts are overrepresented by a factor of 4 among the transcripts that increased in abundance upon ABCE1 KD, suggesting that ABCE1 KD inhibits NMD on a significant fraction of the NMD-sensitive transcripts.

To validate RNA-seq results, we used reverse transcription followed by quantitative PCR (RT-qPCR) to measure the relative RNA levels of a panel of well-characterized NMD-sensitive transcripts in total RNA prepared from HeLa cells with a knockdown of ABCE1, or a knockdown of the central NMD factor UPF1 as a positive control. For HNRNPL, TRA2B, SRSF11 and TMEM208, the NMD-sensitive transcript (labeled _NMD; Figure 1C) arises from an alternative splicing event (intron retention, inclusion of a poised exon or usage of an alternative 5′ or 3′ splice site) as part of an autoregulatory feedback loop and the productively spliced form of the respective pre-mRNA encodes for the full length protein and is not targeted by NMD (labeled _PROT) (76). We included RNA measurements of the _PROT splice forms of these genes as a control and to exclude that the increases observed for the _NMD splice forms were due to changes at the level of transcription or splicing. The RT-qPCR results were in good agreement with the RNA-seq data, confirming the up-regulation of a fraction of the NMD-sensitive transcripts (GADD45B, HNRNPL_NMD and TMEM208_NMD) in ABCE1 KD, while another fraction of NMD-sensitive transcripts (TRA2B_NMD and SRSF11_NMD) was not affected and SMG5 was weakly but not statistically significantly upregulated. Altogether, these data indicated that ABCE1 KD inhibits NMD on a sub-population of NMD-sensitive transcripts, but none of the known NMD-inducing features could readily explain why certain NMD targets were up-regulated by ABCE1 KD while others remained unaffected. To exclude that the observed changes arose from an off-target effect of our siRNA, we repeated the ABCE1 knockdown with two additional siRNA sequences (ABCE1 85 and 86, respectively) and obtained essentially the same result (Supplementary Figure S2).

ABCE1 knockdown also inhibits NMD of well-studied NMD reporter constructs

Since only a sub-population of endogenous NMD targets were upregulated by ABCE1 KD, we wondered whether widely used NMD reporter constructs were also affected by ABCE1 depletion. Therefore, we performed the ABCE1 knockdown in HeLa cells that stably express either of two well-characterized NMD reporters, namely the TCRβ (57) or immunoglobulin-μ (Ig-μ) minigenes (56). Of both reporter genes, there exists a PTC-free (so called 'wild-type') version that produces an mRNA which is not sensitive to NMD (TCRβ WT and miniμ WT), and a version harbouring a PTC in the middle of the coding sequence (TCRβ ter68, miniμ ter310) that strongly triggers NMD (Figure 2A, B, top). Again, our siRNA-based knockdown protocol resulted in a reduction of ABCE1 protein to about 10% of the normally present amount (Figure 2A, B, bottom). Measurements of the respective relative reporter RNA levels by RT-qPCR showed that both NMD-sensitive transcripts increased by 2.5-fold (TCRβ ter68) and 8-fold (miniμ ter310) upon ABCE1 KD, whereas the PTC-free versions remained unchanged (miniμ WT) or even slightly decreased (TCRβ WT) (Figure 2C, D; see also Supplementary Figure S2B, D for miniμ), indicating that NMD of these two reporter transcripts was inhibited by ABCE1 KD. Hence, we reasoned that these reporters would be useful to further investigate how ABCE1 inhibited NMD.

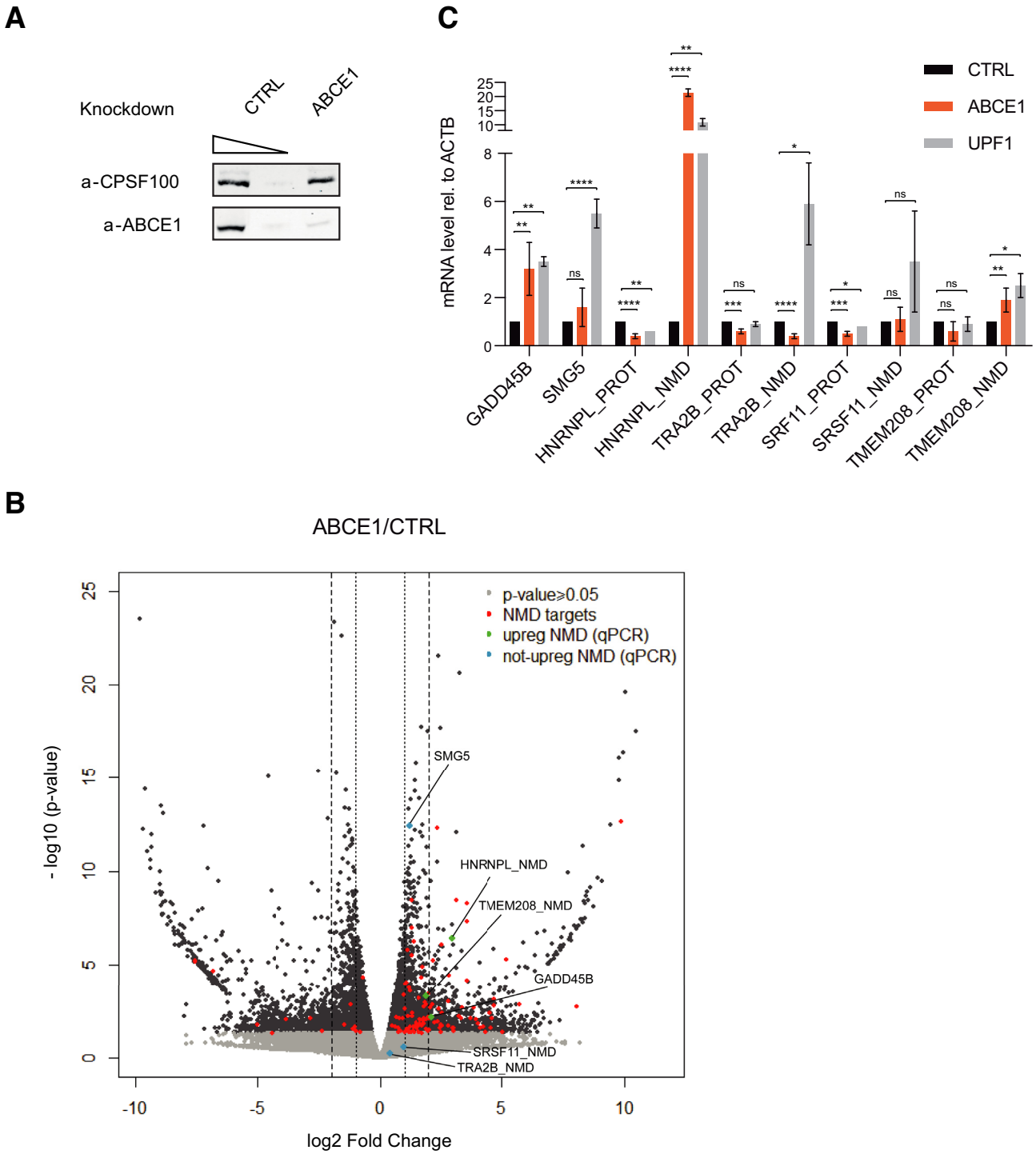

Figure 1. Depletion of ABCE1 inhibits NMD on many NMD-sensitive transcripts. (**A**) Western blot analysis to assess efficacy of ABCE1 knockdown in the samples used for RNA-seq. 100% and 10% of the control knockdown sample (CTRL) and 100% of the ABCE1 KD sample were loaded. CPSF-100 served as loading control. A representative blot of three independently performed experiments is shown. (**B**) Volcano plot showing RNA level changes upon ABCE1 KD from the RNA-seq data along the x-axis and *P*-values for each differential expression value along the y-axis. For each transcript, the average log2 fold change of three replicates for ABCE1 KD compared to control KD is shown. Red dots denote previously identified high confidence NMD targets identified (5), dark and light grey dots show transcripts with and without significant changes (*P*-value ≥ 0,05), respectively. Green and blue dots depict upregulated and not upregulated known NMD targets that were validated by RT-qPCR in (C). The dotted and the dashed lines indicate log2 fold changes of ±1 and ±2, respectively. (**C**) Relative mRNA levels, normalized to β-actin (ACTB), of indicated transcripts were measured by RT-qPCR from total RNA samples of cells with control KD, ABCE1 KD or UPF1 KD. Mean values and standard deviations (SD) of four replicates for ABCE1 KD and 2 replicates for UPF1 KD are shown. *P*-values > 0.05 are indicated as ns (not significant), *$P \leq 0.05$, **$P \leq 0.01$, ***$P \leq 0.001$ and ****$P \leq 0.0001$. Of HNRNPL, TRA2B, SRSF11 and TMEM208, an alternatively spliced NMD-sensitive transcript (NMD) and the NMD-resistant protein coding mRNA (PROT) were measured using splice variant-specific primers. GADD45B and SMG5 are NMD-sensitive mRNAs.

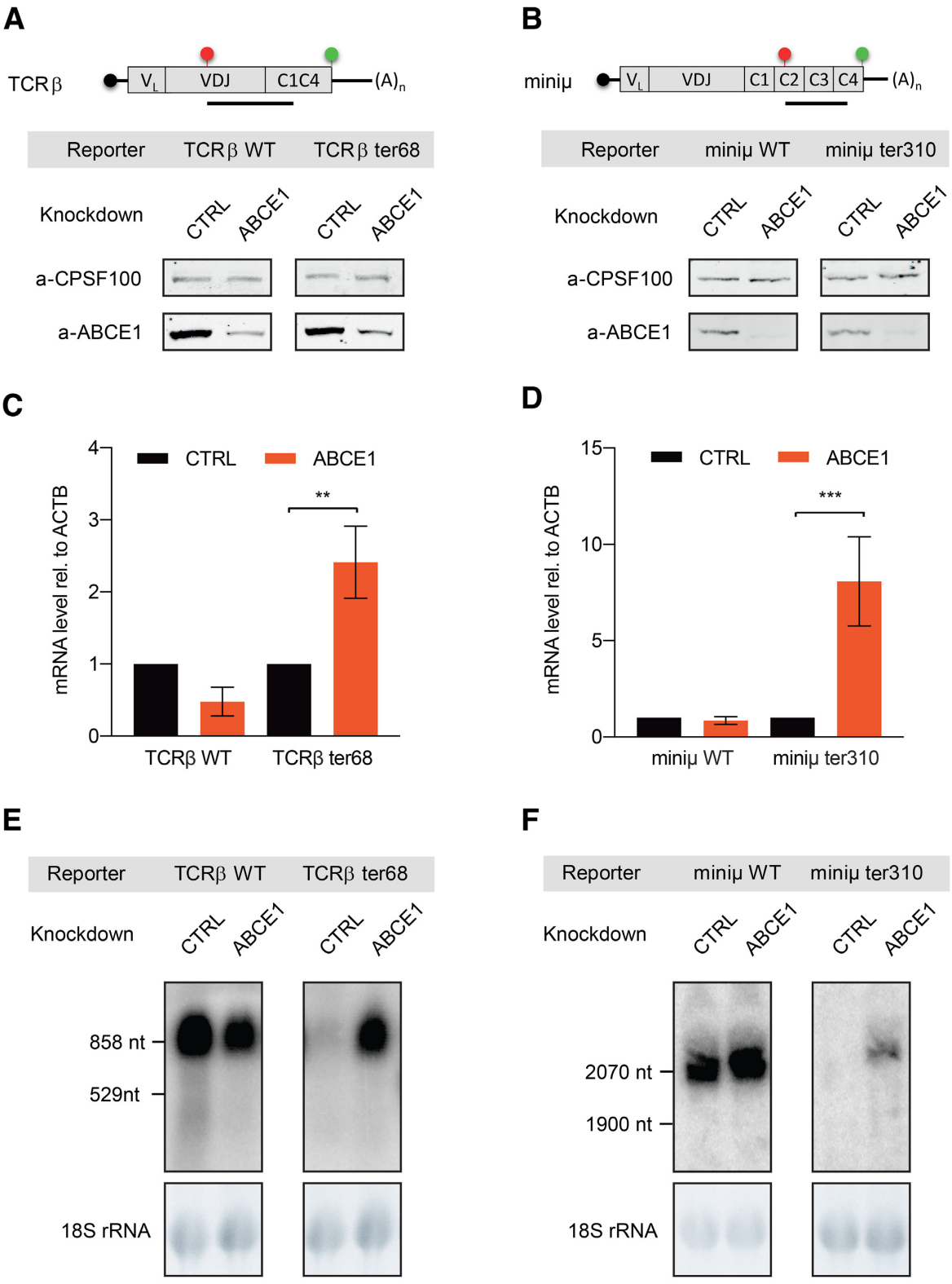

Figure 2. Depletion of ABCE1 increases mRNA levels of NMD-sensitive reporters before SMG6-mediated endonucleolytic cleavage. (**A, B**) Top: Schematic representation of TCRβ and miniμ reporter mRNAs. Red dots indicate the position of premature termination codons (ter68 in TCRβ and ter310 in miniμ), green dots represent the normal termination codon. The position of the probes used for northern blot analysis are indicated as black lines below the constructs. Bottom: Western blot analysis monitoring the efficacy of the ABCE1 KD in HeLa cells stably expressing TCRβ WT or ter68, and miniμ WT or ter310, respectively. CPSF-100 served as loading control. Representative blots of three independently performed experiments are shown. (**C, D**) Relative levels of TCRβ or miniμ mRNA, normalized to β-actin (ACTB) mRNA, were measured by RT-qPCR. Mean values and SD of 4 replicates and *P*-values are shown as in Figure 1. (**E, F**) Northern blot analysis of total RNA isolated from HeLa cells expressing TCRβ (WT or ter68) or miniμ (WT or ter310) cells with and without ABCE1 KD. 18S rRNA levels detected from the agarose gel stained with ethidium bromide served as loading control.

ABCE1 knockdown inhibits NMD before the induction of RNA degradation

The observed NMD inhibition of the two NMD reporters TCRβ ter68 and miniμ ter310 prompted us to further investigate at which point in the NMD pathway this inhibition occurs. In yeast, depletion of the ABCE1 homolog Rli1 has been shown to lead to the accumulation of a 3′ RNA decay fragment of an NMD-sensitive mRNA as a consequence of a defect in translation termination (77). The authors of this study speculated that in the absence of Rli1, stalled ribosomes at the premature stop codon would block the 5′-3′ exonuclease Xrn1, resulting in the accumulation of this 3′ RNA decay intermediate. To see whether ABCE1 KD would also cause the appearance of a similar decay intermediate in human cells, we examined by northern blot WT and PTC-containing TCRβ and miniμ transcripts expressed in HeLa cells (Figure 2E, F). For both transcripts, we used probes that hybridize to the RNA downstream the PTC, which allows the detection of both the full-length transcript and the putative 3′ fragment (Figure 2A, B, top). While the NMD-insensitive WT versions of TCRβ and miniμ mRNAs did not change significantly as expected, we detected a marked increase of the full-length transcripts of the NMD-sensitive versions (TCRβ ter68 and miniμ ter310) upon ABCE KD (Figure 2E, F). However, in contrast to yeast, no 3′ decay intermediates were detected, indicating that in human cells, ABCE1 depletion inhibits NMD at an earlier step, before the initiation of RNA degradation, which usually occurs by a SMG6-mediated endonucleolytic cleavage.

NMD-sensitive mRNAs are strongly associated with polysomes in ABCE1-depleted cells

Since NMD is dependent on active translation (78,79), we next examined whether ABCE1 depletion might inhibit NMD indirectly by causing a global translation inhibition. Notably, a previous study has reported that ABCE1 KD in human cells reduces the general translation level (80). To assess the overall translation activity in control and ABCE1 KD cells, we pulse-chased HeLa cells with puromycin and detected puromycylated nascent polypeptide chains using an antibody against puromycin (Figure 3A). The western blot results revealed a decrease of total protein synthesis by ∼40% in cells depleted of ABCE1. However, this overall reduction in protein synthesis is unlikely to account for the selective inhibition of NMD on a fraction of the NMD targets, and moreover the puromycylation assay does not address which step of translation is affected by ABCE1 KD. There is evidence that ABCE1 depletion causes ribosome stalling at termination codon and an increased ribosome occupancy in the 3′ UTR, suggesting mainly an impairment of translation termination (44,45,47). According to this model, mRNAs are expected to still be associated with polysomes upon ABCE1 KD, and strong association of mRNAs with polysomes would provide indirect evidence that these mRNAs are still actively translated. To test this hypothesis, we knocked down ABCE1 in HeLa cells (Figure 3B, top) and performed polysome profiling (Figure 3B, bottom) to assess the association of different transcripts with monosomes (M) and polysomes (P) (Figure 3C). The relative distribution between the monosome and the polysome fractions were quantified by RT-qPCR for two NMD-sensitive (HNRNPL_NMD, TMEM208_NMD) and two NMD-insensitive (HNRNPL_PROT, TMEM208_PROT) endogenous transcripts. Remarkably, compared to the control, the association of the NMD-sensitive transcripts HNRNPL_NMD and TMEM208_NMD with polysomes was not decreased under ABCE1 KD, similar to the protein coding isoforms that are actively translated under control and KDs conditions. We conclude that, even though ABCE1 KD reduces overall the translation rate in cells, this cannot account for the inhibition of NMD on these transcripts, since they are still actively translated as judged by their association with polysomes.

Depletion of ABCE1 induces ribosome stalling at termination codon and an enrichment in 3′ UTR ribosome occupancy

To gain more insight about translation changes and ribosome occupancy at TCs in the absence of ABCE1, we performed ribosome profiling in HeLa cells in which ABCE1 was knocked down as described before (Supplementary Figure S3A) using a modified version of the protocol published by Ingolia and coworkers (63). In contrast to commonly used ribosome profiling protocols, the use of cyclohexemide (CHX) was avoided, because CHX does not prevent disassembly of ribosomes located at TCs. Instead, cells were flash-frozen with liquid nitrogen, which has been shown to block elongating ribosomes as well as ribosomes located at TCs (21). Moreover, the use of CHX can bias the final output of ribosome footprints, as it seems to allow slow, concentration-dependent elongation prior to lysis according to recent studies (81,82). The experiment was conducted in triplicates with ABCE1 KD and Control KD cells and the mapped reads showed overall strong 3 nucleotide periodicity, confirming that most of them indeed represent ribosome-protected RNA fragments (Supplementary Figure S3B). Ribosome occupancy was examined by dividing the transcripts into four regions (5′ UTR, CDS from the start codon to the middle, CDS from the middle to the TC, and 3′ UTR) and aligning ribosome-derived reads to each specific region, relative to the total number of reads (Supplementary Figure S3C). While ribosome occupancy in the 5′ UTR was low and very similar between ABCE1 KD and Control KD, a slightly lower ribosome coverage in the CDS was detected in ABCE1 KD compared to Control KD (Supplementary Figure S3C), indicating overall reduced translation and confirming the results of the puromycylation experiment (Figure 3A). On the contrary, on average more ribosomes appear to be present in 3′ UTR in the ABCE1 KD compared to Control KD, indicating that depletion of ABCE1 increases the rate of TC readthrough and/or translation re-initiation. These results are in agreement with other studies that have observed ribosome stalling at TCs and an increased ribosome occupancy in the 3′ UTR upon ablation of ABCE1 (44,45,47).

To minimize the probability of falsely assigning ribosome-protected fragments (RPFs) that originate from overlapping CDSs of alternative transcript isoforms to the TC and the 3′ UTR, we followed a recently published strategy (73) and chose a single transcript for genes with multiple annotated coding transcripts. Initially, all

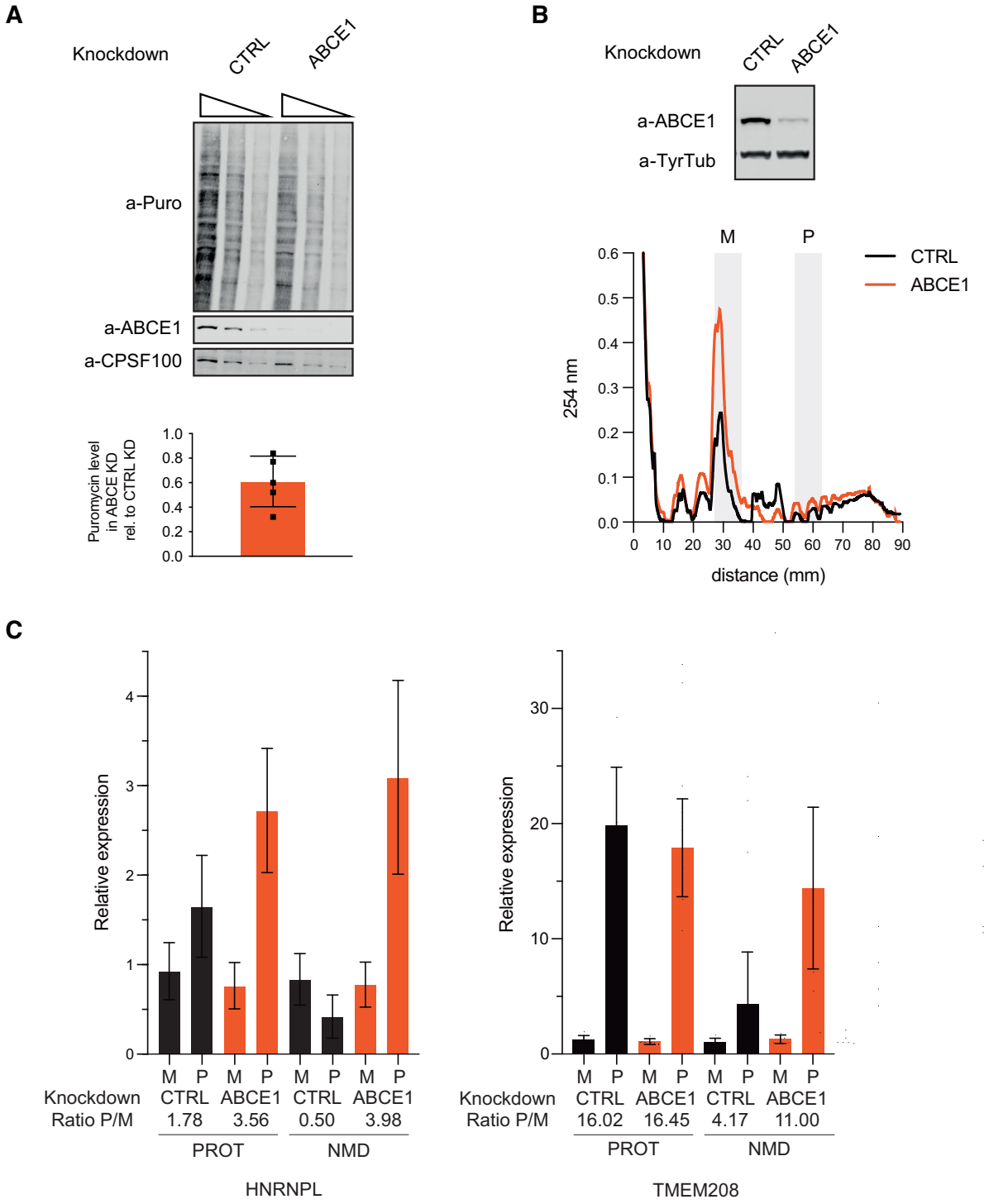

Figure 3. NMD-sensitive mRNAs are associated with polysomes in ABCE1 depleted cells. (**A**) Overall translation activity in cells with and without ABCE1 KD was measured using the SUnSET technique that incorporates puromycin in newly synthesized proteins (59). 100%, 50% and 25% of each protein extract were loaded on an SDS-PAGE, transferred to a nitrocellulose membrane and probed with antibodies against puromycin, ABCE1 and CPSF100 to monitor translation activity, ABCE1 knockdown efficacy and equal loading, respectively. The blot is representative of 5 independently performed experiments, of which the incorporated puromycin in ABCE1 KD samples relative to Control KD samples was quantified and plotted (below). (**B**) Top: Western blot of HeLa lysates to assess efficacy of the ABCE1 knockdown in the samples used for the polysome profiling experiments. Tyrosine Tubulin (TyrTub) served as loading control. The blot is representative of three independently performed experiments. Bottom: Polysome profiles of lysates from cells without (CTRL) or with ABCE1 KD. Similar results were obtained in three independently performed experiments. The fractions corresponding to monosomes (M) and early polysomes (P) (highlighted in grey) were used for RNA isolation and RT-qPCR analysis (C). (**C**) Relative levels of the NMD-sensitive (NMD) and the NMD-insensitive (PROT) isoforms of HNRNPL and TMEM208 RNAs were measured by RT-qPCR in the monosome (M) and polysome (P) fraction and ratios between the polysome and monosome fractions of each condition is depicted. Mean values and standard deviations of three independent experiments are shown.

transcripts with the 3′-most TC were selected and for genes with multiple transcripts sharing this TC, the primary APPRIS transcript was selected (74). This second filtering step resulted in one transcript for almost all genes (99.3%). For the remaining 874 genes whose transcripts did not have an APPRIS score, one transcript isoform was selected randomly. This approach resulted in a total of 12 401 transcripts which were used for further analysis. To obtain more detailed information about ribosome occupancy at TCs and in the 3′ UTR, we performed a metagene analysis of the RPFs in the range between 300 nucleotides upstream of the TC and 100 nucleotides downstream of the ABCE1 KD and the Control KD (Figure 4A, B, top). While average ribosome occupancy at the TC seemed to be the same for ABCE1 KDs and Control KDs, an increased ribosome occupancy in the ABCE1 depleted cells was observed 30 nucleotides upstream of the TC and in the first 100 nucleotides of the 3′ UTR (Figure 4A, B, top), suggestive of disome accumulation at TCs and increased readthrough, respectively. As revealed by the heatmap, ribosome occupancy, and by inference translation of the ∼12 000 transcripts, was affected differently by the depletion of ABCE1 (Figure 4A, B, bottom). When ordered according to ribosome coverage at the TC in ABCE1 KD (Figure 4A, bottom), ∼25% of the transcripts exhibited marked ribosome stalling at the TC compared to Control KD (top section labeled by green line), while more than half of the transcripts showed decreased ribosome occupancy throughout the CDS and at the TC, gradually decreasing to a level at which no ribosomes were detected anymore at the TC (bottom section labeled by red line). The combination of these two effects explains why in the metagene analysis, no difference in ribosome occupancy at the TC was visible between ABCE1 KD and Control KD. By contrast, the increased ribosome occupancy in the 3′ UTR in the metagene analysis was also clearly visible when individual transcripts were analyzed and ordered according to ribosome coverage in the 3′ UTR in the ABCE1 KD dataset (Figure 4B, bottom). Interestingly, of the 2000 transcripts with the most ribosomes in the 3′ UTR (Figure 4B, top section labeled by yellow line), one quarter also showed a concomitant higher ribosome coverage in the CDS. Therefore, to exclude that the increase of ribosome coverage in the 3′ UTR was simply due to a general high engagement of ribosomes with these specific transcripts, the ribosome-protected reads mapping in the 3′ UTR were normalized to the average ribosome occupancy in the CDS (Figure 4C). Confirming our previous notion, ABCE1 KD exhibited elevated ribosome occupancy in the 3′ UTR, even when scaled to ribosome occupancy in CDS, supporting the hypothesis that ABCE1 depletion might create an environment favourable for readthrough or re-intiation events. To exclude that the observed differences in ribosome engagement simply correlated with mRNA abundance, total RNA-seq data from the cells used for the ribosome profiling experiments were analyzed (Supplementary Figure S3D). When all transcripts together were assessed, no overall change in mRNA levels was detected between ABCE1 KD and CTRL KD conditions (Supplementary Figure S3D, All) and the same was true when different sub-populations of transcripts were analyzed separately: the 2000 transcripts presenting the highest ribosome occupancy at the TC in ABCE1 KD cells (High Stop; group labeled with green line in Figure 4A), the 2000 mRNAs showing the lowest ribosome occupancy at the TC (Low Stop; group labeled with red line in Figure 4A), and the 2000 transcripts presenting the highest ribosome occupancy in the 3′ UTR in ABCE1 KD cells (High 3′-UTR; group labeled with yellow line in Figure 4B). This analysis shows an overall similar pattern of mRNA expression changes between the different groups (Supplementary Figure S3D, left). Moreover, the mRNA levels of transcripts with a low ribosome occupancy at TC and in the CDS (Low Stop) are similar to all transcripts considered in the analysis in the ABCE1 KD condition (All), demonstrating that their low engagement with ribosomes is not simply due to a low abundance of these transcripts (Supplementary Figure S3D, right).

TC readthrough has been reported previously as a mechanism that can suppress NMD (36). Therefore, we checked where the previously identified endogenous NMD-sensitive transcripts (5) were located in the heatmaps shown in Figure 4A and B. When ribosome occupancy at the TC was considered, NMD targets were distributed homogeneously throughout the entire heatmap, being present in both the top (green) as well as the bottom (red) group (Figure 4A). It therefore seems that ribosome stalling in the absence of ABCE1 occurs neither preferentially nor specifically on NMD targets, consistent with the observation that the mRNA levels of only a fraction of NMD targets was upregulated in ABCE1 KD (Figure 1).

We next tried to search for those NMD targets upregulated in ABCE1 KD (identified in the RNA-seq experiment, Figure 1B) in the green and red groups of transcripts, but because several of them share most of their sequence with the corresponding protein-coding isoform, unambiguous transcript identification was not possible with the exception of the NMD-sensitive SMG5-encoding mRNA, which consists of a single isoform: It belongs to the top 2000 transcripts with a high ribosome occupancy in the 3′ UTR (Figure 4B, section labeled by the yellow line). To still look at NMD targets separately and compare it to other transcripts that are insensitive to NMD, the ribosome occupancy in 3′ UTRs, relative to CDS, was analyzed as before (Figure 4C), this time comparing the NMD targets against the rest of the transcripts (Figure 4D). As already indicated by the heatmaps, higher ribosome occupancy in the 3′ UTR was detected in both transcript categories. On NMD targets, translating ribosomes in 3′ UTR can prevent NMD activation. However, since ribosome profiling does not inform if the ribosome-protected RNA fragments detected in the 3′ UTR originate from continued translation after a readthrough event, from ribosomes that have re-initiated translation, or if they represent translationally inactive ribosomes without any peptide chain associated, we addressed this question using reporter genes.

ABCE1 KD promotes in-frame and out-of-frame readthrough

We noted that among the endogenous NMD targets (5) that we detected in our RNA-seq, UGA was the most frequently occurring TC. Among these transcripts, the occur-

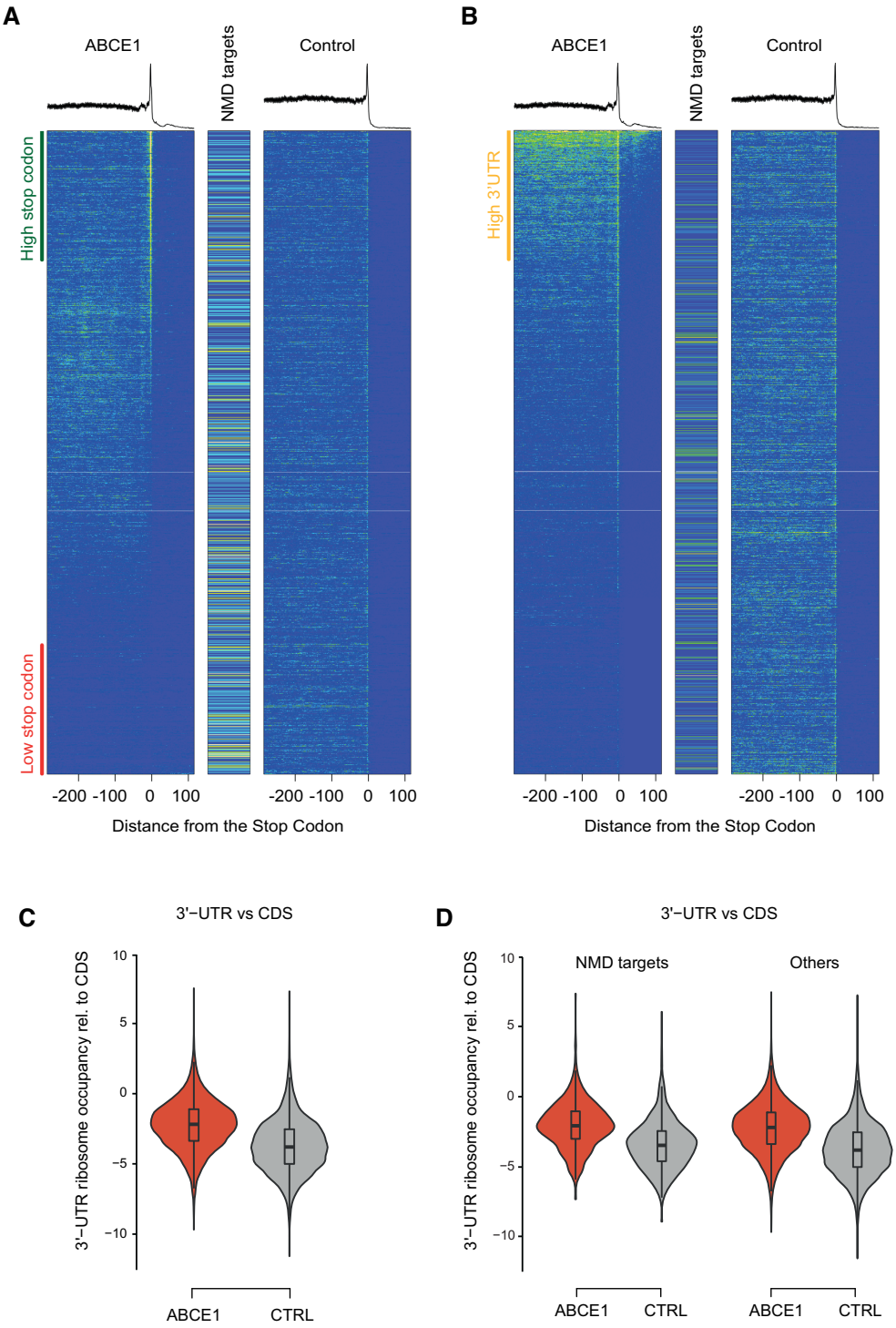

Figure 4. Enrichment of ribosome occupancy at termination codon and in the 3′ UTR in ABCE1 depleted cells. (**A**) Top: Metagene analysis of ribosome-protected footprints from ABCE1 KD (left) or control KD (right). 12 401 transcripts were aligned to the stop codon and mapped reads from 300 nucleotides upstream to 100 nucleotides downstream of the stop codon are shown. Bottom: Heatmap of ribosome-derived reads of all the transcripts considered for the metagene analysis, ordered according to their ribosome occupancy at the stop codon under ABCE1 KD. The 2000 transcripts with the highest ribosome occupancy at the stop codon (green line) and the 2000 transcripts with the lowest ribosome coverage at stop codon (red line) are indicated. Previously identified NMD-sensitive transcripts (5) are depicted with a bright line between the heatmap panels. Each pixel corresponds to 10 transcripts. (**B**) Top: Metagene analysis of ribosome coverage as in A. Bottom: Heatmap of ribosome-derived reads as in A, this time ordered according to their ribosome occupancy in the 3′ UTR under ABCE1 KD. The 2000 transcripts with the highest ribosome occupancy in the 3′ UTR are marked with a yellow line. The position of the NMD-sensitive transcripts in the heatmap is indicated as in A. (**C**) Analysis of mean ribosome occupancy in the 3′ UTR relative to mean ribosome occupancy in CDS. For each replicate, the ratio between the RPFs in the 3′ UTR and in the CDS was determined, then averaged and log transformed. *P*-values were calculated using Anova statistic test ($P \leq$ 1e–16). (**D**) Analysis of mean ribosome occupancy in the 3′ UTR as in C, but performed separately for NMD-sensitive transcripts and all other transcripts (Anova statistic test for 'NMD targets' and for 'Others'; $P \leq$ 1e–16).

rence of the UGA TC was even further enriched among the sub-population of endogenous NMD targets that was upregulated upon ABCE1 KD: ∼82% of them have UGA as the stop codon compared to 55% of the endogenous NMD targets that were not upregulated under ABCE1 depletion. According to previous studies, UGA is the least efficiently recognized stop codon of the three canonical stop codons, resulting in the highest readthrough rates (83). Because of the overrepresentation of the UGA stop codon among our ABCE1-dependent NMD targets, and since insertion of readthrough-promoting retroviral RNA elements into NMD reporter transcripts has been shown to antagonize UPF1 binding to their 3′ UTR and subsequent RNA decay (36), we hypothesized that increased translational readthrough could suppress NMD on the NMD targets that were upregulated upon ABCE1 KD. Notably, increased readthrough upon ABCE1 KD would also be consistent with previous findings in yeast (84). To measure readthrough, we used a well-established readthrough reporter gene (25) in which the ORFs for Renilla luciferase (Rluc) and Firefly luciferase (Fluc) are positioned either in frame or separated by one of the three stop codons (Figure 5A). The Fluc/Rluc ratio serves as a measure to quantify readthrough of stop codons under different conditions. First, we tested readthrough efficiency in cells transiently transfected with the dual-luciferase reporter and treated with geneticin (G418), an aminoglycoside antibiotic that promotes readthrough (85). Consistent with previous reports (86,87), basal readthrough frequency was lowest with UAA and somewhat higher with UAG and UGA. After treatment of the cells with 400 μg/ml G418 for 24 h, readthrough increased at each of the three stop codons, with UGA being the most permissive, reaching about 2.5% readthrough (Supplementary Figure S4A). When we measured readthrough occurrence under Control KD and ABCE1 KD conditions (Figure 5B), we observed increased readthrough at all three stop codons upon ABCE1 depletion (Figure 5C). ABCE1 KD caused the strongest increase in readthrough at the UAA stop codon, with UAA and UGA reaching 0.4% and 0.5% readthrough, respectively, while UAG was read through with about 0.7% efficiency. This result demonstrates that ABCE1 KD increases readthrough frequency in HeLa cells, consistent with previous findings (83). That the readthrough frequency in ABCE1 KD increased to a similar level with all three TCs, while G418 increased readthrough at the different TCs to different levels (compare Figure 5C with Supplementary Figure S4A), is consistent with our TC usage analysis performed on the ribosome profiling data (Supplementary Figure S4B): The ratio of the three TCs was similar among the previously described sub-populations of transcripts (High Stop, Low Stop and High 3′ UTR; see Figure 4A, B and Supplementary Figure S3D).

Because the reads from the Ribo-seq that mapped to the 3′ UTR in the ABCE1 KD samples did not have a strong 3 nucleotide periodicity, we hypothesized that the readthrough observed under ABCE1 depletion might frequently be associated with a frameshift, causing the ribosome to ensue translation out of the original reading frame. To test if such frameshift-associated readthrough of the TC indeed occurs, we introduced into the dual luciferase reporter gene an additional nucleotide downstream of the TC that separates the Rluc CDS from the Fluc CDS (Figure 5D). In order to translate Fluc in this reporter, the ribosome either needs to read through the Rluc TC and concomitantly shift the reading frame, or ribosomes would have to re-initiate translation at the Fluc start codon. Upon knockdown of ABCE1 (Figure 5E), we observed an increase of readthrough in the +1 frame under ABCE1 depletion (Figure 5F). Notably, the Fluc/Rluc ratio with the frameshift constructs was higher than with the original dual luciferase reporters (Figure 5, compare C and F), which most probably is due to the altered TC context. While the TC is followed by GAT in the original reporters (Figure 5A), it is followed by AGA in the +1 constructs (Figure 5D), and it is known that the three sequence of the three nucleotides downstream of the TC influence how well the TC is recognized during translation (38). The occurrence of readthrough-coupled frameshifting could in fact explain the NMD inhibition for several of the endogenous NMD targets that are upregulated in ABCE1 KD (Figure 1B). The majority of them has multiple in-frame TCs closely downstream of the NMD-triggering TC, which would quickly stop 'escaping' ribosomes and prevent them from translocating far enough to clear the 3′ UTR of NMD factors. However, in most of the cases, one of the other two frames would allow ribosomes to proceed past the last exon-exon junction, where termination is expected to no longer trigger NMD. We therefore postulate that the readthrough events on the endogenous NMD targets frequently are accompanied by a frameshift of the ribosome.

To further assess if readthrough can explain the observed NMD inhibition under ABCE1 KD, we looked for readthrough in an NMD-sensitive transcript. The miniμ NMD reporter was ideal for this, because of a polyclonal antibody that with high affinity and specificity recognizes the constant region of the encoded mouse Ig-μ heavy chain. Western blotting was performed with lysates from cells stably expressing miniμ WT or ter310 mRNA and treated with control or ABCE1 siRNAs, or with G418 (Figure 5G). While full-length Ig-μ was readily detected in comparable amounts in miniμ WT-expressing cells under all conditions, as expected, truncated Ig-μ chains were detected in cells expressing miniμ ter310. As a consequence of increased miniμ ter310 mRNA due to NMD inhibition upon ABCE1 KD or G418 treatment, the amount of truncated Ig-μ chains increased (compare lane 5 with lanes 6 and 7). Most importantly, in miniμ ter310-expressing cells depleted for ABCE1 or treated with G418, full-length Ig-μ chains were also detected in addition to the truncated ones, indicating that under these conditions, a sizable fraction of the ribosomes read through the PTC and translated all the way down to the normal termination codon, thereby presumably displacing UPF1, EJCs and other NMD-inducing factors from the region downstream of the PTC. Consistent with the occurrence of frameshift-associated readthrough events, additional bands were detected specifically under ABCE1 depletion in miniμ ter310 expressing cells (Figure 5G, lane 6) which migrate slightly higher the truncated one. Based on their size, they most likely represent such out-of-frame readthrough events in which the ribosome runs into TCs downstream the PTC. Noteworthy, the detection of

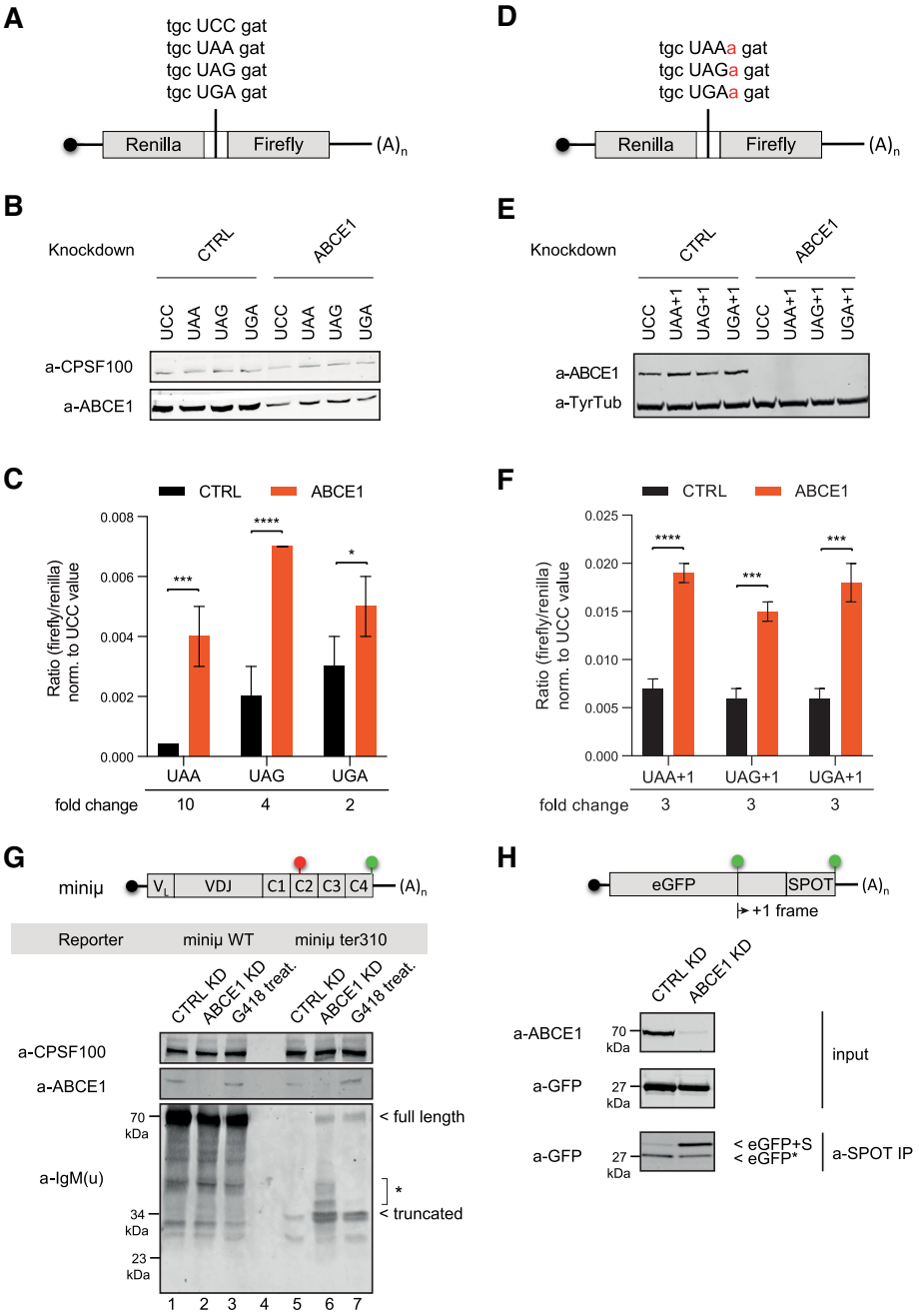

Figure 5. ABCE1 KD promotes frameshift-prone TC readthrough. (**A**) Schematic representation of the dual luciferase readthrough reporter construct. (**B**) Western blot analysis to assess efficacy of ABCE1 knockdown in cells expressing the different readthrough reporter constructs. CPSF-100 served as loading control. A representative blot of three independently performed experiments is shown. (**C**) The ratios between Firefly and Renilla luciferase activities were determined for each of the three the stop codon-containing reporters (UAA, UAG, UGA) in cells with a control or ABCE1 KD and set relative to the ratio measured with the no-stop reporter (UCC), representing the percentage of readthrough at the three different stop codons. Mean values and SD from three independent experiments and *P*-values are shown as in Figure 1. (**D**) Schematic representation of the modified dual luciferase readthrough reporter constructs, in which the Firefly luciferase reading frame was shifted by 1 nucleotide relative to the Renilla luciferase reading frame. (**E**) Assessment of ABCE1 KD efficacy in cells expressing the frameshifted dual luciferase reporter constructs as in (**B**), except that that tyrosine tubulin served as loading control. (**F**) The frameshifted dual luciferase readthrough reporter constructs were expressed and the ratios between Firefly and Renilla luciferase activities were determined as in (**C**), depicting the Firefly/Renilla ratios of the frameshifted constructs as a percentage of the ratio measured with the no-stop reporter. (**G**) Ig-μ protein detection by western blotting of miniμ-expressing HeLa cells depleted of ABCE1 or after G418 treatment using a polyclonal antibody against the constant region of Ig-μ (C1vC4). Bands corresponding to truncated (translation termination at ter310) and full-length Ig-μ protein are indicated. Based on their size range, the bands denoted with an asterisk most likely represent truncated Ig-μ chains resulting from out-of-frame readthrough events of ter310. CPSF-100 served as loading control and the efficacy of ABCE1 depletion was also assessed. The blot is representative of three independently performed experiments with similar results. (**H**) Detection of the out-of-frame readthrough product eGFP+S (eGFP with a C-terminal SPOT tag in the +1 frame) by western blotting of protein immunoprecipitated with anti-SPOT nanobody (a-SPOT IP) from cell lysates with control or ABCE1 KD and detected with anti-GFP antibody (a-GFP). eGFP* depicts unspecifically co-precipitated eGFP, which is highly abundant in the lysate (see input, a-GFP panel). Efficacy of the ABCE1 KD was monitored in the input samples.

full-length Ig-μ chains in miniμ ter310-expressing ABCE1-depleted cells suggests that ABCE1 not only functions in splitting and recycling of the small and large ribosomal subunits, but that it also may play a role in polypeptide release during translation termination.

While the results obtained with the frame-shifted dual luciferase reporter (Figure 5D) suggested increased readthrough-coupled frameshifting (Figure 5F) in the absence of ABCE1, we could not exclude the possibility that the increased Fluc activity might result from translation reinitiation rather than readthrough. To obtain unambiguous evidence for frameshift-associated readthrough, we therefore tested an eGFP reporter construct encoding in the +1 frame a C-terminal SPOT tag (Figure 5H and Supplementary Figure S4C). After immunoprecipitation (IP) with an anti-SPOT nanobody from lysates of ABCE1-depleted cells, SPOT-tagged eGFP was easily detected by western blotting using an anti-eGFP antibody (Figure 5H; band labeled eGFP+S). A very weak signal for this frameshift-associated readthrough product was also seen in the IP of the control KD cells, and under both conditions, similar amounts of the much more abundant normally terminated eGFP protein co-precipitated unspecifically (band labelled eGFP*). Noteworthy, while we could detect out-of-frame readthrough with this reporter (Figure 5H), we did not detect any in-frame readthrough product after IP with anti-FLAG antibody (Supplementary Figure S4C, D), suggesting that the sequence context around the TC might affect in which frame translation continues past the TC.

Depletion of ABCE1 leads to ribosome collision on highly translated transcripts

Stop codon readthrough associated with frameshifting has not been reported so far, but recently it was shown in yeast that ribosome collisions in the CDS result in +1 frameshifting in the absence of No-Go Decay (55). According to their model, transcripts with high ribosome density are more sensitive to frameshifting events, because ribosome collisions occur more frequently on these transcripts. That ribosome collision is a marker for recognition of aberrant translation and activation of ribosome quality control (RQC) has also been strongly indicated by recent work characterizing the ubiquitin ligase ZNF598 as a sensor for collided ribosomes (51). We hypothesized that ribosome collisions might also be the mechanism causing the observed TC readthrough (with or without frameshifting) in the absence of ABCE1. Therefore, we scrutinized our ribosome profiling data for evidence of ribosome collisions at TCs or of the presence of disome formation at TCs. Although our ribosome profiling protocol involved the isolation of monosomes and hence cannot detect disomes, we observed in the trace of the metagene analysis and specific for the ABCE1 KD a 'bump' approximately 30 nucleotides upstream of the TC peak (Figure 4A, B, top), which represents the accumulation of a ribosome immediately adjacent to ribosome located at the TC, and the distance from the TC matches with that recently reported for collided ribosomes (49).

Since only a subgroup of transcripts showed a pronounced increase of ribosomes in the 3′ UTR under ABCE1 KD (Figure 4B, High 3′ UTR), we re-analyzed the ribosome occupancy around the TC of the 3000 transcripts with the highest ribosome occupancy in the 3′ UTR. Metagene analysis of the ribosome-protected footprints ranging between 300 nucleotides upstream and 100 nucleotides downstream of the TC of these transcripts revealed overall a higher ribosome occupancy in the CDS, at TC and in the 3′ UTR in the ABCE1 depleted cells compared to the control (Figure 6A). This increased ribosome occupancy under ABCE1 KD is consistent with the suggested ribosome stalling at the TC, which in turn might lead to ribosome queuing in front of the TC and occasional pushing of a ribosome past the TC, where it will continue translation into the 3′ UTR in any of the three frames. As expected for frequent out-of-frame readthrough events, the ribosome-protected footprints mapped to the 3′ UTR did not show a clear periodicity.

To test our hypothesis that under ABCE1 depletion highly translated transcripts were more prone to ribosome collisions at TC and ribosomes being pushed into the 3′ UTR, we determined the ribosome density for the transcripts used in Figure 6A by normalizing the ribosome-protected footprints for each gene relative to the mRNA abundance and CDS length. As suspected, transcripts with higher ribosome occupancy in the 3′ UTR also showed slightly higher ribosome density (Supplementary Figure S5B), suggesting that high ribosome density in the CDS could contribute to increase ribosome collision and more readthrough events. A caveat with Ribo-seq data is, that it cannot distinguish if the detected ribosomes are really actively translating or if they are in a translationally inactive state. To measure actual protein synthesis, we therefore also performed a metabolic labelling with a methionine analogue (L-azidohomoalanine, AHA) in control or ABCE1 KD cells. After the labelling, newly synthesized proteins were enriched and analyzed by mass spectrometry. Consistent with the puromycin incorporation assay (Figure 3A), ABCE1 depletion caused a reduction in newly synthesized proteins (Supplementary Figure S5C, TAMRA), but did not affect the overall protein levels of the cell (Supplementary Figure S5C, SYPRO). To assess if the transcripts with high ribosome occupancy in the 3′ UTR are also highly translated, we compared the Ribo-seq data with the results of the AHA-labeling experiment. For this comparison, we considered the top 1000 transcripts from the 'High 3′ UTR' group (Supplementary Figure S5A) and proteins that exhibited a high normalized spectral abundance factor (NSAF) in ABCE1 KD sample in the AHA-experiment. Since detection of peptides derived from specific protein isoforms by mass spectrometry is difficult, the analysis was performed at gene level, considering unique gene ID from the Ribo-seq transcripts with high ribosome occupancy into the 3′ UTR ($n = 1000$) and unique protein ID from the AHA-experiment ($n = 1372$). About the 33% of the genes ($n = 334$) with high ribosome occupancy in the 3′ UTR were also highly translated in ABCE1 depleted cells (Supplementary Figure S5D). Altogether, these results support the idea that it might be colliding ribosomes at TC that cause readthrough by pushing the stalled ribosome into the 3′ UTR, where it can ensue translation stochastically in presumably any of the three frames.

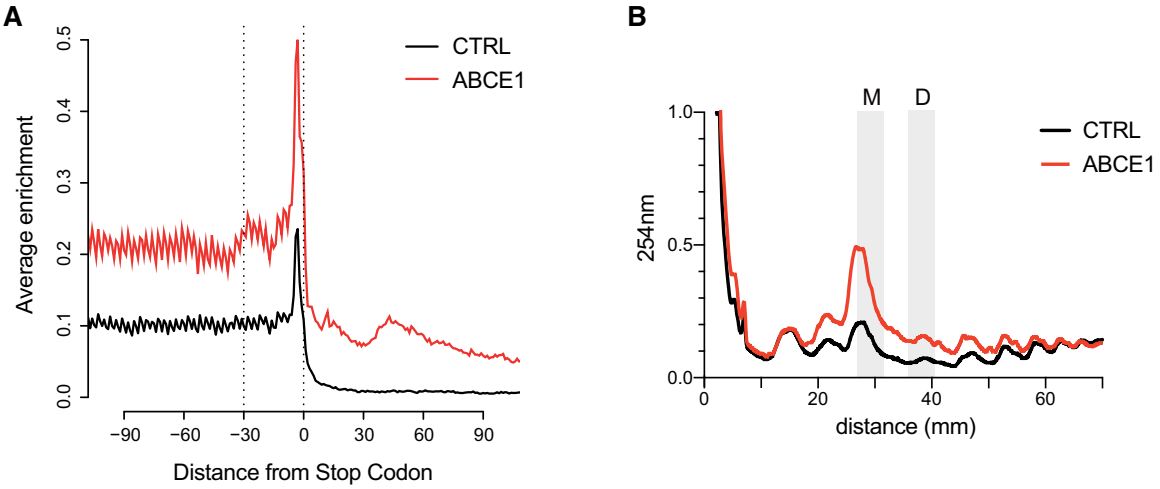

C

Protein	Uniprot	Monosome NSAF Ratio ABCE1/CTRL	Disome NSAF Ratio ABCE1/CTRL	Monosome Ubiquitin Ratio ABCE1/CTRL	Disome Ubiquitin Ratio ABCE1/CTRL
RPS3	P23396	1.5	1.5	4.8	2.1
RPS27A	P62979	1.0	0.9	0.2	0.4
RACK1	P63244	1.7	1.5	0.4	0.8
ZNF598	Q86UK7	1.2	1.5	0.0	0.0
ERF1	P62495	2.3	4.8	0.0	0.0
ABCE1	P61221	0.5	0.0	0.0	0.0

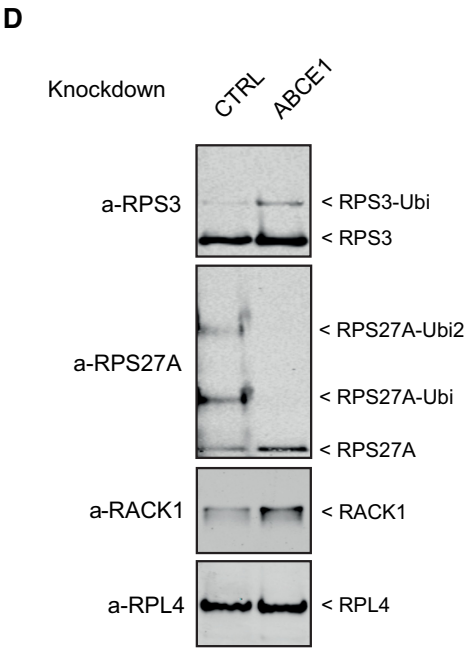

Figure 6. ABCE1 KD promotes ribosome collision and RQC activation. (**A**) Metagene analysis of ribosome-protected footprints from control and ABCE1 KD. Transcripts were aligned to the stop codon and mapped reads from 300 nucleotides upstream to 100 nucleotides downstream of the stop codon are shown. The Top 3'000 transcripts with the highest ribosome occupancy in the 3′ UTR in the ABCE1 KD were included in the analysis (see heatmap in Figure 4B). (**B**) Polysome profiles of lysates from cells with control or ABCE1 KD. Fractions corresponding to monosomes (M) or disomes (D) (highlighted in light grey) were used for protein isolation and mass spectrometric analysis. (**C**) The mass spectrometry (MS) data for a subgroup of proteins involved in RQC is depicted. The average of the ratio of the normalized spectral abundance factor (NSAF) for each protein between ABCE1 KD and control KD is shown, averaged from two independent experiments. Monosome and disome fractions were analyzed separately. For the analysis of ubiquitinated proteins, the ubiquitin modification was detected by MS, an average ubiquitin-modification score was calculated for each protein and the ratio of this score between ABCE1 KD and control KD is shown. A value of 0.0 indicates that no ubiquitination was detected. (**D**) Validation of MS results by western blotting of proteins extracted from the monosome fractions obtained in the polysome profiling experiments (B). Antibodies against RPS3 and RPS27A detect both non-ubiquitinated as well as mono- and di-ubiquitinated forms of the respective protein. RPL4 served as loading control.

Activation of ribosome quality control (RQC) in ABCE1 depleted cells

While the detection of ribosome collision *in vivo* is technically very challenging, recent reports have pointed out a connection between ribosome collision and the activation of RQC. In particular, collided disomes were shown to be the structural entity recognized by the E3 ubiquitin ligase Hel2/ZNF598 (49,51). Ubiquitination of several ribosomal proteins was reported as a consequence of ZNF598 recruitment to aberrant translation events, activating the RQC cascade (52,54). One well-documented example is the ribosomal protein RPS3, which is ubiquitinated by ZNF598 when ribosomes stall on a poly(A) stretch (49,52,54). Moreover, the ribosome associated protein RACK1 also seems to play a crucial role in ZNF598-dependent RQC activation (54). To obtain more evidence that ribosome collisions occur frequently in cells lacking ABCE1, we knocked down ABCE1 in HeLa cells and performed polysome profiling (Figure 6B) to subsequently assess ubiquitination of proteins isolated from the monosome or disome fractions. Compared to the control KD, we found in the monosome and disome fractions of the ABCE1 KD a significant increase in RPS3 ubiquitination and a strong decrease of ubiquitinated RPS27A, while the overall abundance of both proteins remained unchanged (Figure 6C, D). The RPS27A gene encodes a fusion protein consisting of ubiquitin at the N-terminus and ribosomal protein S27a at the C-terminus and the ubiquitin moiety serves as substrate for ubiquitination of other proteins. Therefore, reduction of ubiquitinated RPS27A indicates an elevated need for ubiquitin, for example to modify other ribosomal proteins in RQC or to target misfolded newly synthesized proteins to the proteasome. Moreover, the release factor eRF1 was elevated in monosomes and disomes of the ABCE1 depleted cells, suggesting that eRF1-bound ribosomes cannot recycle properly when ABCE1 is not available (Figure 6C). Likewise, also RACK1 was enriched in monosomes and disomes of ABCE1 depleted cells, further supporting the idea of RQC activation in the absence of proper ribosome recycling (Figure 6C, D). Collectively, these results suggest that in the absence of ABCE1, RQC is activated as a consequence of ribosome collisions at the TC, which is sensed by ZNF598 and leads to the ubiquitination of RPS3 (and probably additional ribosomal proteins), similar to what has been reported to occur when ribosomes collide inside the CDS or within poly(A) stretches.

DISCUSSION

The ribosome recycling factor ABCE1 has so far been shown to be required for splitting apart the large and small ribosomal subunits after translation termination (39) and under conditions of limiting amounts of eRF3 to stimulate eRF1-mediated peptide release (84). Here, we show that ABCE1 and correct recycling of ribosomes is also needed for triggering NMD on many NMD-sensitive mRNAs. We report that depletion of ABCE1 suppresses NMD of a subgroup of NMD-sensitive mRNAs in HeLa cells (Figure 1) and of two well-established NMD reporters (i.e. TCRβ and miniμ) (Figure 2A–D). According to a previous study, the conditional depletion of the yeast orthologue of ABCE1, Rli1 causes ribosome stalling at the termination codon (TC), blocking degradation on NMD targets and leading to the stabilization of degradation-intermediates for NMD-sensitive mRNAs (77). Although NMD shares similarities between yeast and human cells, we only detected an increase of full-length RNA with the two NMD reporter genes TCRβ and miniμ under ABCE1 KD (Figure 2E, F), indicating that ABCE1 depletion inhibits NMD at a step prior to SMG6-mediated endonucleolytic cleavage. Since ABCE1 has been reported to function in translation termination and in the first steps of translation initiation (39), its depletion is expected to affect overall protein synthesis, which in turn might cause the observed NMD inhibition, since NMD is strictly translation-dependent (3). However, although overall protein synthesis was reduced by ∼40% in ABCE1 depleted cells (Figure 3A), this cannot account for the observed NMD inhibition. First, under ABCE1 KD conditions, NMD-sensitive mRNAs were found strongly enriched in polysomes (Figure 3B, C), and secondly, protein products were detected for the miniμ reporter gene (Figure 5G), excluding the possibility that NMD inhibition induced by ABCE1 depletion might simply result from an overall translation inhibition.

Readthrough has been previously reported to antagonize NMD by displacing UPF1 from the 3′ UTR of NMD reporter transcripts (36). While rare readthrough events still allowed for UPF1 re-association with the RNA, frequent readthrough led to a marked decrease of steady-state UPF1 interaction with the 3′ UTR and inhibited NMD (36). If the mere clearing of NMD factors from the 3′ UTR by elongating ribosomes was sufficient to spare an mRNA from NMD, this could happen both by readthrough of the TC as well as by re-initiation of post-termination ribosomes downstream of the TC. Interestingly, in the absence of Rli1/ABCE1, an increase of ribosome occupancy in the 3′ UTR and re-initiation events have been reported in yeast and in anucleate platelets and reticulocytes (45,47). Our results corroborate the idea of readthrough or re-initiation leading to NMD inhibition, as our ribosome profiling experiments detected increased ribosome occupancy in the 3′ UTR of a substantial fraction of mRNAs in ABCE1 depleted cells, including many NMD-sensitive mRNAs (Figure 4). Indeed, full-length protein was detected from the PTC-harboring miniμ mRNA only in cells depleted for ABCE1 or when treated with a readthrough-promoting drug (G418), demonstrating that a fraction of the stalled ribosomes read through the PTC without releasing the nascent polypeptide and continue translation all the way to the normal TC (Figure 5G). While for the miniμ NMD reporter, these readthrough events can explain the NMD inhibition, one would have to postulate a slightly different mechanism to explain how the endogenous NMD targets that are upregulated in ABCE1 KD escape NMD, because the majority of them contains several in-frame TCs closely downstream of the NMD-triggering TC, which would quickly stop again 'escaping' ribosomes and prevent them from translocating far enough into the 3′ UTR to clear the 3′ UTR of NMD factors. However, in most of the cases, one of the other two frames would allow translation to proceed past the last exon-exon junction, where termination is predicted to no longer trigger NMD. Supporting this idea of frameshift-prone readthrough, ABCE1 KD increased not

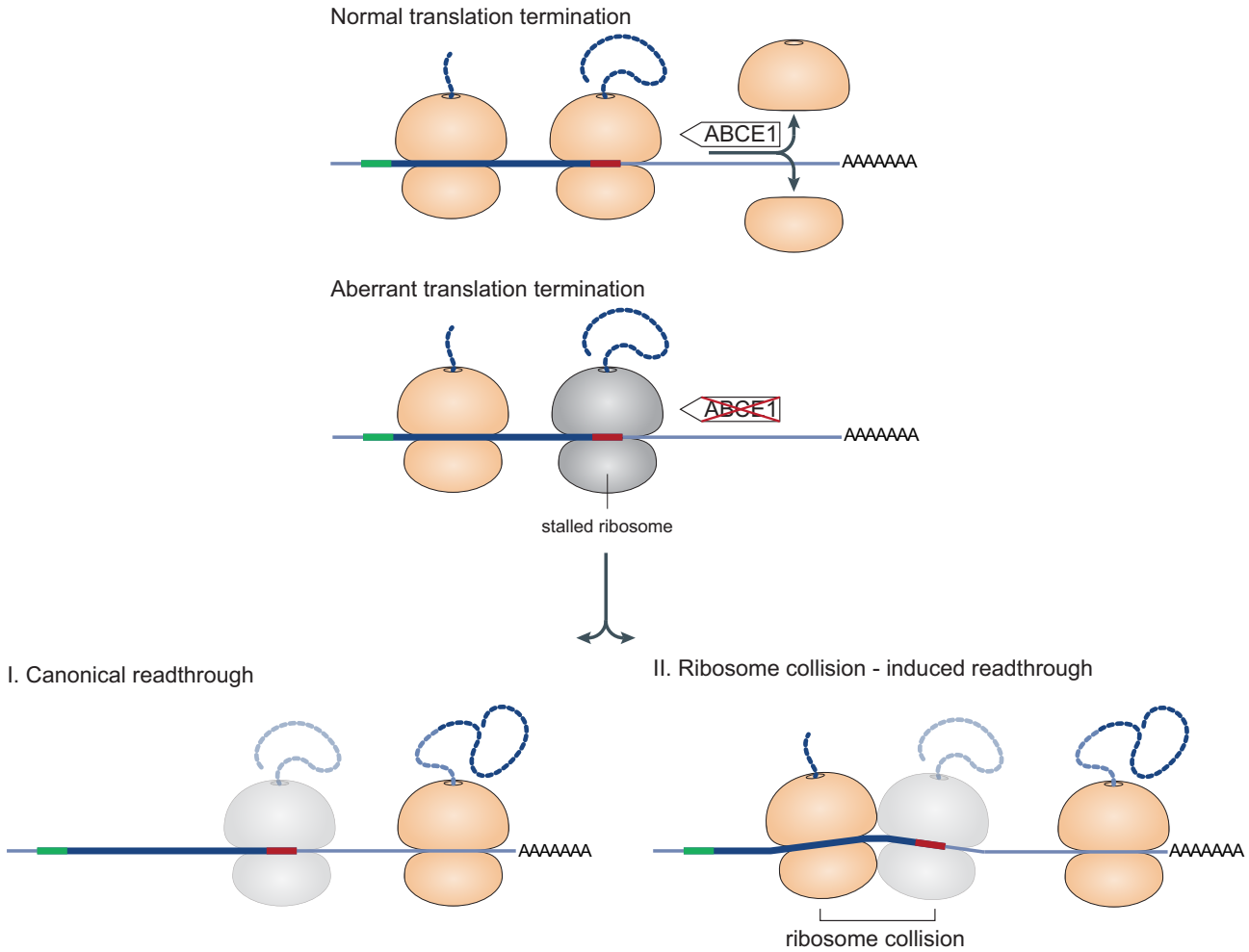

Figure 7. Model for two different modes of stop codon readthrough under limiting ABCE1 concentrations. During normal translation termination, disassembly and recycling of the ribosomal subunits is promoted by ABCE1 after stop codon recognition and release of the nascent peptide chain. In the absence of ABCE1, ribosomes fail to terminate properly and stall at the stop codon for prolonged time. Prolonged stalling of a ribosome at the stop codon on the one hand increases the chance for the binding of a near-cognate tRNA leading to canonical readthrough. On the other hand, this also increases the probability of the following ribosome to run into stalled ribosome and collectively our data suggests that this leads to a ribosome collision-induced push of the terminating ribosome into the 3′ UTR, where it can resume translation in any of the three frames. Start and stop codons are depicted in green and red, the CDS and the encoded protein chain are shown in dark blue, while the 3′ UTR and any peptide sequence encoded therein are depicted in light blue.

only in-frame but also out-of-frame readthrough in a dual luciferase readthrough reporter (Figure 5A–F), and in a GFP reporter designed to specifically detect readthrough coupled with a +1 frameshift (Figure 5H). These results in combination with detecting in the Ribo-seq experiments the specific accumulation of a second ribosome immediately upstream of the one located at the TC when ABCE1 was depleted (Figures 4 and 6A; the 'bump' at position −30) led us postulate that the readthrough events promoted by ABCE1 depletion could be caused by a ribosome collision pushing the stalled ribosome at the TC into the 3′ UTR, where it would resume translation randomly in any of the three reading frames (Figure 7; and see below). Ribosome collisions occurring within the CDS and on poly(A) stretches have been shown recently to activate the ribosome quality control (RQC) pathway, of which the ZNF598-mediated ubiquitination of ribosomal proteins is a hallmark (49,52,54). Consistent with a related mechanism underlying the herein reported frameshift-prone TC readthrough under limiting ABCE1 concentrations, increased RPS3 ubiquitination and an enrichment of ZNF598 and RACK1 were detected in monosomes and disomes of ABCE1 KD cells (Figure 6B–D).

It is currently not understood how ABCE1 depletion leads to readthrough and why under this condition the nascent polypeptide does not get efficiently released. According to our current understanding of translation termination, ribosome recycling at the TC is expected to occur after polypeptide release, preventing readthrough and translation into the 3′ UTR (88). Yet our ribosome profiling results showed clearly an increase of ribosome occupancy at the TC in ABCE1 KD cells, as well as an enrichment of ribosome coverage in the 3′ UTR (Figure 4A, B), consistent with previous studies (44,45,47). However, not only termination seems to be affected in the absence of ABCE1, as about 25% of all transcripts analyzed in the ribosome

profiling are almost completely devoid of ribosomes (Figure 4A, section marked by red line), suggesting that translation of these transcripts basically ceased when ABCE1 became limiting. In contrast, transcripts with a high ribosome occupancy in the 3′ UTR tend to also have more ribosomes in the CDS (this applies to 4% of all analyzed transcripts; Figure 4B). As aforementioned, the metagene analysis of ribosome occupancy revealed an accumulation of ribosome-protected reads 30 nucleotides upstream the TC exclusively in the ABCE1 depleted cells (Figure 6A), which most likely represent ribosomes positioned contiguously behind the ribosome stalled at the TC. This signal at −30 nucleotides is also clearly visible in the heatmap on the fraction of transcripts that exhibits the strongest ribosome stalling at the TC (Figure 4A, top section denoted by the green line) and supports the idea of a ribosome traffic jam on specific mRNAs under ABCE1 depletion as a consequence of improper ribosome clearing at the TC. Prolonged stalling at the TC increases the chance for a ribosome to read through the TC or to re-initiate translation downstream of the TC if the nascent peptide has already been released. Since the transcripts showing a −30 nucleotide 'bump' do not all have increased ribosome occupancy in the 3′ UTR, it seems that we may have captured two different outcomes of ABCE1 KD: on a fraction of the transcripts, ribosomes accumulate immediately upstream of the ribosome stalled at the TC, while on another transcript population, ribosomes strongly accumulate in the CDS, at TC and in the 3′ UTR. While on the former group of transcripts, ribosomes seem to be stuck at the TC but the translation rate on these transcripts is low, which prevents the pileup of ribosomes along the CDS, the latter group might represent a traffic jam of ribosomes that accumulate on heavily translated transcripts because of delayed release at the TC. We hypothesize that some ribosomes stalled at the TC might read through the TC by incorporating a near-cognate tRNA (Figure 7, canonical readthrough), whereas others will be pushed into the 3′ UTR by a following ribosome running into the one stalled at the TC (Figure 7, ribosome collision-induced readthrough). It seems plausible that in the second scenario, the forward pushed ribosome could resume translation in another frame depending on the strength of the push, the sequence context around the TC and where the next cognate tRNA binds the A-site, which would explain for many of the endogenous NMD targets that are upregulated in the ABCE1 KD how their 3′ UTR might be cleared of NMD-inducing factors. Moreover, the traffic jam model might also explain the heterogeneous ribosome distribution across all transcripts, with a group of transcripts being highly translated and a fraction of mRNAs almost devoid of ribosomes, since the highly translated transcripts might sequester a sizable fraction of the ribosomes, thereby preventing their recycling and association with other mRNAs. It was reported that the intracellular abundance of the release factor eRF1 plays a crucial role in TC recognition and readthrough (38), and limiting eRF1 availability by trapping it on ribosomes stalled at TCs of a subset of mRNAs could lead to enhanced readthrough on other transcripts. The fact that we observed readthrough without peptide release—i.e. full-length protein production—under ABCE1 KD could also be the result of such a sequestering of eRF1. A scenario in which eRF1 is trapped at TCs in the ABCE1 KD and its concentration becomes limiting for other translation termination events, is supported by the detection of increased amounts of eRF1 associated with monosomes and disomes under limiting ABCE1 concentrations (Figure 6C).

Ribosome collision has thus far been mainly investigated in the context of RQC activation due to ribosome stalling in poly(A) stretches (49,52,54). However, ribosome collisions were recently also induced at TCs using the inactive eRF1-AAQ mutant in an *in vitro* translation system (51), suggesting that RQC might also occur as a result of aberrant translation termination. Even though the direct detection of collided ribosomes *in vivo* remains elusive, we provide here for the first time evidence for RQC activation under limiting ABCE1 concentrations in mammalian cells by detecting increased ubiquitination of RPS3 and an increase of ribosome-associated RACK1 (Figure 6), strongly indicating a role for RQC triggered by colliding ribosomes in resolving problems with translation termination.

Further research will be required to elucidate the molecular links between translation termination, NMD and RQC and to fully understand the consequences of ribosome collisions happening at stop codons. To this end, a recently developed method that allows measuring translation termination events in real-time on single mRNA molecules (89) provides a powerful tool to shed light on the translation and translation termination dynamics of different mRNAs under different conditions. Based on recent work (90) and the data presented here, it seems clear that ABCE1 will turn out to be a key player in regulating ribosome release from TCs and connecting translation termination to surveillance systems such as NMD and RQC.

DATA AVAILABILITY

The high throughput Illumina sequencing data sets (Ribo-seq and total RNA-seq) are available at Gene Expression Omnibus (GEO) website under the series ID GSE143301 (https://www.ncbi.nlm.nih.gov/geo/query/acc.cgi?acc=GSE143301). This series comprises the 18 files GSM4256659 to GSM4256676.

Weblinks to bioinformatics software tools:

cutadapt: https://cutadapt.readthedocs.io/en/stable/index.html
bowtie2: http://bowtie-bio.sourceforge.net/bowtie2/index.shtml
Salmon: https://salmon.readthedocs.io/en/latest/index.html

SUPPLEMENTARY DATA

Supplementary Data are available at NAR Online.

ACKNOWLEDGEMENTS

We are grateful to Martino Colombo for initial bioinformatics analyses and thank Evan Karousis, Andrea Eberle, Sofia Nasif and Lukas Gurzeler for thoughtful comments.

FUNDING

NCCR RNA & Disease funded by the Swiss National Science Foundation (SNSF); SNSF [31003A-162986, 310030B-182831]; canton of Bern. Funding for open access charge: Swiss National Science Foundation.
Conflict of interest statement. None declared.

REFERENCES

1. Lykke-Andersen,J. and Bennett,E.J. (2014) Protecting the proteome: eukaryotic cotranslational quality control pathways. *J. Cell Biol.*, **204**, 467–476.
2. Shoemaker,C.J. and Green,R. (2012) Translation drives mRNA quality control. *Nat. Struct. Mol. Biol.*, **19**, 594–601.
3. Karousis,E.D. and Muhlemann,O. (2019) Nonsense-mediated mRNA decay begins where translation ends. *Cold Spring Harb. Perspect. Biol.*, **11**, a032862.
4. Behm-Ansmant,I. and Izaurralde,E. (2006) Quality control of gene expression: a stepwise assembly pathway for the surveillance complex that triggers nonsense-mediated mRNA decay. *Genes Dev.*, **20**, 391–398.
5. Colombo,M., Karousis,E.D., Bourquin,J., Bruggmann,R. and Muhlemann,O. (2017) Transcriptome-wide identification of NMD-targeted human mRNAs reveals extensive redundancy between SMG6- and SMG7-mediated degradation pathways. *RNA*, **23**, 189–201.
6. Hurt,J.A., Robertson,A.D. and Burge,C.B. (2013) Global analyses of UPF1 binding and function reveal expanded scope of nonsense-mediated mRNA decay. *Genome Res.*, **23**, 1636–1650.
7. Mendell,J.T., Sharifi,N.A., Meyers,J.L., Martinez-Murillo,F. and Dietz,H.C. (2004) Nonsense surveillance regulates expression of diverse classes of mammalian transcripts and mutes genomic noise. *Nat. Genet.*, **36**, 1073–1078.
8. Tani,H., Imamachi,N., Salam,K.A., Mizutani,R., Ijiri,K., Irie,T., Yada,T., Suzuki,Y. and Akimitsu,N. (2012) Identification of hundreds of novel UPF1 target transcripts by direct determination of whole transcriptome stability. *RNA Biol*, **9**, 1370–1379.
9. Viegas,M.H., Gehring,N.H., Breit,S., Hentze,M.W. and Kulozik,A.E. (2007) The abundance of RNPS1, a protein component of the exon junction complex, can determine the variability in efficiency of the nonsense mediated decay pathway. *Nucleic Acids Res.*, **35**, 4542–4551.
10. Wittmann,J., Hol,E.M. and Jack,H.M. (2006) hUPF2 silencing identifies physiologic substrates of mammalian nonsense-mediated mRNA decay. *Mol. Cell. Biol.*, **26**, 1272–1287.
11. Yepiskoposyan,H., Aeschimann,F., Nilsson,D., Okoniewski,M. and Muhlemann,O. (2011) Autoregulation of the nonsense-mediated mRNA decay pathway in human cells. *RNA*, **17**, 2108–2118.
12. Nagy,E. and Maquat,L.E. (1998) A rule for termination-codon position within intron-containing genes: when nonsense affects RNA abundance. *Trends Biochem. Sci.*, **23**, 198–199.
13. Buhler,M., Steiner,S., Mohn,F., Paillusson,A. and Muhlemann,O. (2006) EJC-independent degradation of nonsense immunoglobulin-mu mRNA depends on 3′ UTR length. *Nat. Struct. Mol. Biol.*, **13**, 462–464.
14. Eberle,A.B., Stalder,L., Mathys,H., Orozco,R.Z. and Muhlemann,O. (2008) Posttranscriptional gene regulation by spatial rearrangement of the 3′ untranslated region. *PLoS Biol.*, **6**, e92.
15. Singh,G., Rebbapragada,I. and Lykke-Andersen,J. (2008) A competition between stimulators and antagonists of Upf complex recruitment governs human nonsense-mediated mRNA decay. *PLoS Biol.*, **6**, e111.
16. Stalder,L. and Muhlemann,O. (2008) The meaning of nonsense. *Trends Cell Biol.*, **18**, 315–321.
17. Le Hir,H., Gatfield,D., Izaurralde,E. and Moore,M.J. (2001) The exon-exon junction complex provides a binding platform for factors involved in mRNA export and nonsense-mediated mRNA decay. *EMBO J.*, **20**, 4987–4997.
18. Le Hir,H., Izaurralde,E., Maquat,L.E. and Moore,M.J. (2000) The spliceosome deposits multiple proteins 20–24 nucleotides upstream of mRNA exon-exon junctions. *EMBO J.*, **19**, 6860–6869.
19. Gehring,N.H., Lamprinaki,S., Kulozik,A.E. and Hentze,M.W. (2009) Disassembly of exon junction complexes by PYM. *Cell*, **137**, 536–548.
20. Carlevaro-Fita,J., Rahim,A., Guigo,R., Vardy,L.A. and Johnson,R. (2016) Cytoplasmic long noncoding RNAs are frequently bound to and degraded at ribosomes in human cells. *RNA*, **22**, 867–882.
21. Ingolia,N.T., Lareau,L.F. and Weissman,J.S. (2011) Ribosome profiling of mouse embryonic stem cells reveals the complexity and dynamics of mammalian proteomes. *Cell*, **147**, 789–802.
22. Calviello,L., Mukherjee,N., Wyler,E., Zauber,H., Hirsekorn,A., Selbach,M., Landthaler,M., Obermayer,B. and Ohler,U. (2016) Detecting actively translated open reading frames in ribosome profiling data. *Nat. Methods*, **13**, 165–170.
23. Amrani,N., Ganesan,R., Kervestin,S., Mangus,D.A., Ghosh,S. and Jacobson,A. (2004) A faux 3′-UTR promotes aberrant termination and triggers nonsense-mediated mRNA decay. *Nature*, **432**, 112–118.
24. Peixeiro,I., Inacio,A., Barbosa,C., Silva,A.L., Liebhaber,S.A. and Romao,L. (2011) Interaction of PABPC1 with the translation initiation complex is critical to the NMD resistance of AUG-proximal nonsense mutations. *Nucleic Acids Res.*, **40**, 1160–1173.
25. Ivanov,P.V., Gehring,N.H., Kunz,J.B., Hentze,M.W. and Kulozik,A.E. (2008) Interactions between UPF1, eRFs, PABP and the exon junction complex suggest an integrated model for mammalian NMD pathways. *EMBO J.*, **27**, 736–747.
26. Kashima,I., Yamashita,A., Izumi,N., Kataoka,N., Morishita,R., Hoshino,S., Ohno,M., Dreyfuss,G. and Ohno,S. (2006) Binding of a novel SMG-1-Upf1-eRF1-eRF3 complex (SURF) to the exon junction complex triggers Upf1 phosphorylation and nonsense-mediated mRNA decay. *Genes Dev.*, **20**, 355–367.
27. Muhlemann,O. and Lykke-Andersen,J. (2010) How and where are nonsense mRNAs degraded in mammalian cells? *RNA Biol.*, **7**, 28–32.
28. Cho,H., Han,S., Choe,J., Park,S.G., Choi,S.S. and Kim,Y.K. (2013) SMG5-PNRC2 is functionally dominant compared with SMG5-SMG7 in mammalian nonsense-mediated mRNA decay. *Nucleic Acids Res.*, **41**, 1319–1328.
29. Loh,B., Jonas,S. and Izaurralde,E. (2013) The SMG5-SMG7 heterodimer directly recruits the CCR4-NOT deadenylase complex to mRNAs containing nonsense codons via interaction with POP2. *Genes Dev.*, **27**, 2125–2138.
30. Nicholson,P., Gkratsou,A., Josi,C., Colombo,M. and Muhlemann,O. (2018) Dissecting the functions of SMG5, SMG7, and PNRC2 in nonsense-mediated mRNA decay of human cells. *RNA*, **24**, 557–573.
31. Neu-Yilik,G., Raimondeau,E., Eliseev,B., Yeramala,L., Amthor,B., Deniaud,A., Huard,K., Kerschgens,K., Hentze,M.W., Schaffitzel,C. *et al.* (2017) Dual function of UPF3B in early and late translation termination. *EMBO J.*, **36**, 2968–2986.
32. Muhlrad,D. and Parker,R. (1999) Aberrant mRNAs with extended 3′ UTRs are substrates for rapid degradation by mRNA surveillance. *RNA*, **5**, 1299–1307.
33. Pulak,R. and Anderson,P. (1993) mRNA surveillance by the Caenorhabditis elegans smg genes. *Genes Dev.*, **7**, 1885–1897.
34. Behm-Ansmant,I., Gatfield,D., Rehwinkel,J., Hilgers,V. and Izaurralde,E. (2007) A conserved role for cytoplasmic poly(A)-binding protein 1 (PABPC1) in nonsense-mediated mRNA decay. *EMBO J.*, **26**, 1591–1601.
35. Silva,A.L., Ribeiro,P., Inacio,A., Liebhaber,S.A. and Romao,L. (2008) Proximity of the poly(A)-binding protein to a premature termination codon inhibits mammalian nonsense-mediated mRNA decay. *RNA*, **14**, 563–576.
36. Hogg,J.R. and Goff,S.P. (2010) Upf1 senses 3′UTR length to potentiate mRNA decay. *Cell*, **143**, 379–389.
37. Keeling,K.M., Lanier,J., Du,M., Salas-Marco,J., Gao,L., Kaenjak-Angeletti,A. and Bedwell,D.M. (2004) Leaky termination at premature stop codons antagonizes nonsense-mediated mRNA decay in S. cerevisiae. *RNA*, **10**, 691–703.
38. Cridge,A.G., Crowe-McAuliffe,C., Mathew,S.F. and Tate,W.P. (2018) Eukaryotic translational termination efficiency is influenced by the 3′ nucleotides within the ribosomal mRNA channel. *Nucleic Acids Res.*, **46**, 1927–1944.
39. Gerovac,M. and Tampe,R. (2019) Control of mRNA translation by versatile ATP-Driven machines. *Trends Biochem. Sci.*, **44**, 167–180.
40. Mancera-Martinez,E., Brito Querido,J., Valasek,L.S., Simonetti,A. and Hashem,Y. (2017) ABCE1: a special factor that orchestrates translation at the crossroad between recycling and initiation. *RNA Biol*, **14**, 1279–1285.
41. Heuer,A., Gerovac,M., Schmidt,C., Trowitzsch,S., Preis,A., Kotter,P., Berninghausen,O., Becker,T., Beckmann,R. and Tampe,R. (2017)

Structure of the 40S-ABCE1 post-splitting complex in ribosome recycling and translation initiation. *Nat. Struct. Mol. Biol.*, **24**, 453–460.
42. Guydosh,N.R. and Green,R. (2014) Dom34 rescues ribosomes in 3′ untranslated regions. *Cell*, **156**, 950–962.
43. Mills,E.W. and Green,R. (2017) Ribosomopathies: there's strength in numbers. *Science*, **358**, eaan2755.
44. Sudmant,P.H., Lee,H., Dominguez,D., Heiman,M. and Burge,C.B. (2018) Widespread accumulation of ribosome-associated isolated 3′ UTRs in neuronal cell populations of the aging brain. *Cell Rep.*, **25**, 2447–2456.
45. Young,D.J., Guydosh,N.R., Zhang,F., Hinnebusch,A.G. and Green,R. (2015) Rli1/ABCE1 recycles terminating ribosomes and controls translation reinitiation in 3′UTRs in vivo. *Cell*, **162**, 872–884.
46. Pisarev,A.V., Skabkin,M.A., Pisareva,V.P., Skabkina,O.V., Rakotondrafara,A.M., Hentze,M.W., Hellen,C.U. and Pestova,T.V. (2010) The role of ABCE1 in eukaryotic posttermination ribosomal recycling. *Mol. Cell*, **37**, 196–210.
47. Mills,E.W., Wangen,J., Green,R. and Ingolia,N.T. (2016) Dynamic regulation of a ribosome rescue pathway in erythroid cells and platelets. *Cell Rep.*, **17**, 1–10.
48. Brandman,O. and Hegde,R.S. (2016) Ribosome-associated protein quality control. *Nat. Struct. Mol. Biol.*, **23**, 7–15.
49. Ikeuchi,K., Tesina,P., Matsuo,Y., Sugiyama,T., Cheng,J., Saeki,Y., Tanaka,K., Becker,T., Beckmann,R. and Inada,T. (2019) Collided ribosomes form a unique structural interface to induce Hel2-driven quality control pathways. *EMBO J.*, **38**, e100276.
50. Joazeiro,C.A.P. (2017) Ribosomal stalling during translation: providing substrates for ribosome-associated protein quality control. *Annu. Rev. Cell Dev. Biol.*, **33**, 343–368.
51. Juszkiewicz,S., Chandrasekaran,V., Lin,Z., Kraatz,S., Ramakrishnan,V. and Hegde,R.S. (2018) ZNF598 is a quality control sensor of collided ribosomes. *Mol. Cell*, **72**, 469–481.
52. Juszkiewicz,S. and Hegde,R.S. (2017) Initiation of quality control during Poly(A) translation requires site-specific ribosome ubiquitination. *Mol. Cell*, **65**, 743–750.
53. Simms,C.L., Thomas,E.N. and Zaher,H.S. (2017) Ribosome-based quality control of mRNA and nascent peptides. *Wiley Interdiscip. Rev. RNA*, **8**, doi:10.1002/wrna.1366.
54. Sundaramoorthy,E., Leonard,M., Mak,R., Liao,J., Fulzele,A. and Bennett,E.J. (2017) ZNF598 and RACK1 regulate mammalian ribosome-associated quality control function by mediating regulatory 40s ribosomal ubiquitylation. *Mol. Cell*, **65**, 751–760.
55. Simms,C.L., Yan,L.L., Qiu,J.K. and Zaher,H.S. (2019) Ribosome collisions result in +1 frameshifting in the absence of no-go decay. *Cell Rep.*, **28**, 1679–1689.
56. Buhler,M., Paillusson,A. and Muhlemann,O. (2004) Efficient downregulation of immunoglobulin mu mRNA with premature translation-termination codons requires the 5′-half of the VDJ exon. *Nucleic Acids Res.*, **32**, 3304–3315.
57. Mohn,F., Buhler,M. and Muhlemann,O. (2005) Nonsense-associated alternative splicing of T-cell receptor beta genes: no evidence for frame dependence. *RNA*, **11**, 147–156.
58. Montellese,C., van den Heuvel,J., Ashiono,C., Dorner,K., Melnik,A., Jonas,S., Zemp,I., Picotti,P., Gillet,L.C. and Kutay,U. (2020) USP16 counteracts mono-ubiquitination of RPS27a and promotes maturation of the 40S ribosomal subunit. *eLife*, **9**, e54435.
59. Schmidt,E.K., Clavarino,G., Ceppi,M. and Pierre,P. (2009) SUnSET, a nonradioactive method to monitor protein synthesis. *Nat. Methods*, **6**, 275–277.
60. Eberle,A.B., Lykke-Andersen,S., Muhlemann,O. and Jensen,T.H. (2009) SMG6 promotes endonucleolytic cleavage of nonsense mRNA in human cells. *Nat. Struct. Mol. Biol.*, **16**, 49–55.
61. Zuccotti,P. and Modelska,A. (2016) Studying the translatome with polysome profiling. *Methods Mol. Biol.*, **1358**, 59–69.
62. Aeschimann,F., Xiong,J., Arnold,A., Dieterich,C. and Grosshans,H. (2015) Transcriptome-wide measurement of ribosomal occupancy by ribosome profiling. *Methods*, **85**, 75–89.
63. Ingolia,N.T., Brar,G.A., Rouskin,S., McGeachy,A.M. and Weissman,J.S. (2012) The ribosome profiling strategy for monitoring translation in vivo by deep sequencing of ribosome-protected mRNA fragments. *Nat. Protoc.*, **7**, 1534–1550.
64. Patro,R., Duggal,G., Love,M.I., Irizarry,R.A. and Kingsford,C. (2017) Salmon provides fast and bias-aware quantification of transcript expression. *Nat. Methods*, **14**, 417–419.
65. Soneson,C., Love,M.I. and M.D.,R. (2016) Differential analyses for RNA-seq: transcript-level estimates improve gene-level inferences [version 2; peer review: 2 approved]. *F1000Research*, **4**, 1521.
66. Robinson,M.D., McCarthy,D.J. and Smyth,G.K. (2010) edgeR: a Bioconductor package for differential expression analysis of digital gene expression data. *Bioinformatics*, **26**, 139–140.
67. Martin,M. (2011) Cutadapt removes adapter sequences from high-throughput sequencing reads. *EMBnet.journal*, **17**, 10–12.
68. Zerbino,D.R., Achuthan,P., Akanni,W., Amode,M.R., Barrell,D., Bhai,J., Billis,K., Cummins,C., Gall,A., Giron,C.G. *et al.* (2018) Ensembl 2018. *Nucleic Acids Res.*, **46**, D754–D761.
69. Langmead,B. and Salzberg,S.L. (2012) Fast gapped-read alignment with Bowtie 2. *Nat. Methods*, **9**, 357–359.
70. Love,M.I., Huber,W. and Anders,S. (2014) Moderated estimation of fold change and dispersion for RNA-seq data with DESeq2. *Genome Biol.*, **15**, 550.
71. Durinck,S., Spellman,P.T., Birney,E. and Huber,W. (2009) Mapping identifiers for the integration of genomic datasets with the R/Bioconductor package biomaRt. *Nat. Protoc.*, **4**, 1184–1191.
72. Yu,G. and He,Q.Y. (2016) ReactomePA: an R/Bioconductor package for reactome pathway analysis and visualization. *Mol. Biosyst.*, **12**, 477–479.
73. Wangen,J.R. and Green,R. (2020) Stop codon context influences genome-wide stimulation of termination codon readthrough by aminoglycosides. *eLife*, **9**, e52611.
74. Rodriguez,J.M., Maietta,P., Ezkurdia,I., Pietrelli,A., Wesselink,J.J., Lopez,G., Valencia,A. and Tress,M.L. (2013) APPRIS: annotation of principal and alternative splice isoforms. *Nucleic Acids Res.*, **41**, D110–D117.
75. Ambrosini,G., Dreos,R., Kumar,S. and Bucher,P. (2016) The ChIP-Seq tools and web server: a resource for analyzing ChIP-seq and other types of genomic data. *BMC Genomics*, **17**, 938.
76. Li,Z., Vuong,J.K., Zhang,M., Stork,C. and Zheng,S. (2017) Inhibition of nonsense-mediated RNA decay by ER stress. *RNA*, **23**, 378–394.
77. Serdar,L.D., Whiteside,D.L. and Baker,K.E. (2016) ATP hydrolysis by UPF1 is required for efficient translation termination at premature stop codons. *Nat. Commun.*, **7**, 14021.
78. Carter,M.S., Doskow,J., Morris,P., Li,S., Nhim,R.P., Sandstedt,S. and Wilkinson,M.F. (1995) A regulatory mechanism that detects premature nonsense codons in T-cell receptor transcripts in vivo is reversed by protein synthesis inhibitors in vitro. *J. Biol. Chem.*, **270**, 28995–29003.
79. Thermann,R., Neu-Yilik,G., Deters,A., Frede,U., Wehr,K., Hagemeier,C., Hentze,M.W. and Kulozik,A.E. (1998) Binary specification of nonsense codons by splicing and cytoplasmic translation. *EMBO J.*, **17**, 3484–3494.
80. Toompuu,M., Karblane,K., Pata,P., Truve,E. and Sarmiento,C. (2016) ABCE1 is essential for S phase progression in human cells. *Cell Cycle*, **15**, 1234–1247.
81. Gerashchenko,M.V. and Gladyshev,V.N. (2014) Translation inhibitors cause abnormalities in ribosome profiling experiments. *Nucleic Acids Res.*, **42**, e134.
82. Hussmann,J.A., Patchett,S., Johnson,A., Sawyer,S. and Press,W.H. (2015) Understanding biases in ribosome profiling experiments reveals signatures of translation dynamics in yeast. *PLos Genet.*, **11**, e1005732.
83. Dabrowski,M., Bukowy-Bieryllo,Z. and Zietkiewicz,E. (2015) Translational readthrough potential of natural termination codons in eucaryotes–The impact of RNA sequence. *RNA Biol.*, **12**, 950–958.
84. Shoemaker,C.J. and Green,R. (2011) Kinetic analysis reveals the ordered coupling of translation termination and ribosome recycling in yeast. *Proc. Natl. Acad. Sci. U.S.A.*, **108**, E1392–E1398.
85. Bukowy-Bieryllo,Z., Dabrowski,M., Witt,M. and Zietkiewicz,E. (2016) Aminoglycoside-stimulated readthrough of premature termination codons in selected genes involved in primary ciliary dyskinesia. *RNA Biol.*, **13**, 1041–1050.
86. Loughran,G., Chou,M.Y., Ivanov,I.P., Jungreis,I., Kellis,M., Kiran,A.M., Baranov,P.V. and Atkins,J.F. (2014) Evidence of efficient stop codon readthrough in four mammalian genes. *Nucleic Acids Res.*, **42**, 8928–8938.

87. Manuvakhova,M., Keeling,K. and Bedwell,D.M. (2000) Aminoglycoside antibiotics mediate context-dependent suppression of termination codons in a mammalian translation system. *RNA*, **6**, 1044–1055.
88. Hellen,C.U.T. (2018) Translation termination and ribosome recycling in eukaryotes. *Cold Spring Harb. Perspect. Biol.*, **10**, a032656.
89. Yan,X., Hoek,T.A., Vale,R.D. and Tanenbaum,M.E. (2016) Dynamics of translation of single mRNA molecules in vivo. *Cell*, **165**, 976–989.
90. Nurenberg-Goloub,E. and Tampe,R. (2019) Ribosome recycling in mRNA translation, quality control, and homeostasis. *Biol. Chem.*, **401**, 47–61.